Evaluation of the influence of aerosols on radiative processes and turbulent surface flows within the Aburrá Valley.

Natalia Roldán Henao

Universidad Nacional de Colombia

Facultad de Minas, Escuela de Geociencias y Medio Ambiente

Medellín, Colombia

2020

Evaluation of the influence of aerosols on radiative processes and turbulent surface flows within the Aburrá Valley.

Natalia Roldán Henao

A thesis submitted in partial fulfillment of the requirements for the degree of:

Master of Engineerig in Water Resources

Advisor: PhD. Carlos David Hoyos

Co-advisor: MsC. Laura Herrera-Mejia

Line of research:

Hydroclimatology, Air Quality

Universidad Nacional de Colombia

Facultad de Minas, Escuela de Geociencias y Medio Ambiente

Medellín, Colombia

2020

To my caring and loving parents, Nicolás Roldán and Gloria Henao, who taught me to love science and believe in myself.

Acknowledgments

I especially want to thank my advisor Carlos David Hoyos for his continuous support and teachings during all these years, for trusting me and allowing me to grow both professionally and academically, and also for allowing me to be part of this great family of researchers.

I also want to thank my co-advisor Laura Herrera, for her patience, teachings, and advice while I was working in this thesis.

I thank my SIATA colleagues, especially the Air Quality team. Their support and collaboration were essential in completing this work.

My most profound gratitude to my love Jhayron Pérez, you encourage me at every moment, and gave me your strength, helping me to achieve my goals.

Finally, I want to thank my family and friends who had always believed in me and had given me their love and support at all times, especially when the times got rough.

Evaluación de la influencia de aerosoles en procesos radiativos y flujos superficiales turbulentos dentro del Valle de Aburrá.

Resumen

El Valle de Aburrá, un valle densamente poblado ubicado en Colombia, con una topografía de alta complejidad en la cordillera de los Andes, ha experimentado en los últimos cinco años la aparición de episodios críticos de contaminación atmosférica, caracterizados por un aumento en la concentración de aerosoles. Este estudio combina información en tierra y satelital para estudiar los impactos de los aerosoles troposféricos en la radiación, los flujos de energía, capa límite atmosférica, propiedades de las nubes y precipitación en la escala local (Valle de Aburrá) y regional (Colombia). En el valle de Aburrá, la dispersión y absorción de los aerosoles disminuyen la radiación en superficie hasta más de -40 Wm^{-2}; adicionalmente inhiben los flujos de calor latente y sensible, modificando de esta forma la evolución de la capa límite atmosférica. En Colombia, los efectos de los aerosoles están relacionados con los eventos de quema de biomasa que ocurren anualmente en el norte y el este de Colombia. Dado que cada gota de nube necesita una partícula de aerosol (un núcleo de condensación de la nube) para su activación, los aerosoles en Colombia y el Valle también han modificado las propiedades de las nubes. Este estudio encontró reducciones en el tamaño de las gotas de nubes para diferentes tipos de nubes. También investigamos los impactos de los aerosoles en la nube convectivas, y llegamos a la conclusión de que el proceso de difusión podría retrasarse durante episodios de alta concentración de aerosoles. Evaluamos las interacciones aerosoles-nube-precipitación, encontrando un aumento en los eventos de lluvia por la tarde debido a la presencia de aerosoles. Las modificaciones resultantes en las propiedades meteorológicas del Valle de Aburrá podrían inducir retroalimentaciones positivas que conducirían a mayores aumentos en la concentración de contaminantes.

Palabras clave: aerosoles, capa límite atmosférica, meteorología, radiación, absorción, dispersión, núcleos de condensación de nubes, lluvia..

Abstract

The Aburrá Valley, a densely populated valley in Colombia, with highly complex topography at the Andes mountain range, has experienced during the past five years the onset of several critical air pollution episodes, which are characterized by an increase in aerosol concentration. This study combines ground-based and satellite information to study aerosols' impacts on radiation, energy fluxes, atmospheric boundary layer, clouds properties, and precipitation in a local (Aburrá Valley) and regional (Colombia) scale. In the Aburrá Valley, aerosols' scattering and absorption diminish the surface radiation by as much as -40 Wm^{-2}; they also inhibit the latent and sensible heat fluxes, thus modifying the evolution of the boundary layer. In Colombia, aerosols' effects are linked to the biomass burning events that annually occur to the north and to the east of Colombia. Since every cloud droplet needs an aerosol particle (a cloud condensation nuclei) for activation, aerosols in Colombia and in the Valley have also modified the cloud properties. This study found reductions in cloud droplets' size for different cloud types. We investigated aerosols' impacts on convective clouds, concluding that the diffusion process could be retarded during high aerosol concentration episodes. We assessed the aerosols-cloud-precipitation interactions, finding an increase in afternoon-rainfall events due to aerosols' presence. The resultant modifications in the Aburrá Valley's meteorological properties could induce a positive feedback that leads to greater increases in pollutants' concentration.

key words: aerosols,atmospheric boundary layer, meteorology, radiation, absorption, scattering, cloud condensation nucleis, rainfall.

Content

List of figures

1 Introduction

During the past few years, the increasing rate of aerosols concentration in Colombia's largest cities has gained an important role in the country's scientific and political agendas. The dynamics of large cities, the expansion of the agricultural frontier, and the country's frequent biomass burning events have deteriorated air quality over the years, which is increasingly evident from the increment in suspended particles in the atmosphere.

Medellın, Colombia, and its surrounding metropolitan area in the Aburrá Valley have experienced the onset of critical air-quality episodes during the last five years. These episodes are characterized by poor air quality and, in particular, sudden peaks of PM2.5 concentration. The combination of growing emissions from mobile and biomass burning sources, complex topography, and unfavorable climate and meteorological conditions for the vertical dispersion of pollutants caused PM2.5 concentrations to peak once a year during February and March. March 2016 is now considered one of the most critical and intense events that the city has experienced to date. During this event, hourly particulate matter concentrations reached 180 $\mu g/m^3$, maximum daily concentrations were as high as 118 $\mu g/m^3$, and the city reported 22 days of unhealthy air quality conditions according to the U.S. Environmental Protection Agency (EPA) standards.

Despite the high rates of contamination registered annually in the territory, so far, there were not investigations that seek to understand the effects of atmospheric aerosols on the local and regional meteorology. This study is the first attempt to investigating aerosols' direct and indirect effect over the Aburrá Valley and Colombia's territory. It relies on in situ air-quality

measurements from the official Aburrá Valley network and satellite information from NASA, and it uses a methodology mainly based on statistical assessments.

This work is divided into two chapters. The first one includes an evaluation of the direct radiative effects of aerosols, from the differences in incident solar radiation, energy fluxes, and the atmospheric boundary layer. Additionally, this chapter presents a characterization of aerosols in the Valley, from the perspective of their optical properties and carbonaceous content.

The second chapter corresponds to an evaluation of the aerosol-cloud-precipitation interactions over the Aburrá Valley and Colombia. In this chapter, we rely mainly on clouds' microphysical properties, which are continuously measured from remote sensing from space. We also used ground-based sensors belonging to the Aburrá Valley monitoring network to have information about the aerosols.

This work's central aim was to examine aerosols' direct and indirect effects and their role in sensible heat fluxes and atmospheric boundary layer changes.

2 Aerosols Radiative Effects and Optical Properties Assessment in Colombia and the Aburrá Valley.

2.1. Introduction

In the last decades, air pollutants increased because of anthropogenic activities, such as fuel combustion, industrial processes, nonindustrial fugitive sources, and transportation sources (Seinfeld and Pandis, 2012). Aerosols are among the most important air pollutants worldwide. These correspond to airborne particles, which can be both solid and liquid, and whose size ranges from 0.01 to 100 micrometers. Despite their small mass or volume fractions, atmospheric aerosols strongly influence the transfer of radiant energy and the spatial distribution of latent heating through the atmosphere, affecting the weather and climate (Boucher et al., 2013). According to its chemical composition, and optical properties, they can both heat and cool the Earth's atmosphere, thus becoming the greatest source of uncertainty for global climate change (Boucher et al., 2013). The chemical composition of aerosols emitted by anthropogenic and natural sources includes sulfate, black carbon (BC), organic carbon (OC), mineral dust, and nitrate.

Atmospheric particles interact with solar radiation through dispersion and absorption and, to a minor portion with terrestrial radiation through absorption, scattering, and emission

(Boucher et al., 2013). Sulfate aerosols scatter primarily solar radiation and have a cooling effect of the Earth-atmosphere system (North et al., 2014), by enhancing the total reflected solar radiation from the Earth. Strongly absorbing aerosols, such as black carbon and organics, have a warming effect. Absorbing aerosols reduce the solar radiation reaching the surface, but at the same time, these aerosols absorb the upward solar radiation reflected from below. Therefore, absorbing aerosols counteract the cooling effect of other aerosols at the top of the atmosphere (TOA) (North et al., 2014). Since aerosol emitting sources can be both natural and anthropogenic, Direct Radiative Forcing of Aerosols (DRFA) refers exclusively to the proportion that corresponds to anthropogenic aerosols. At the same time, the Direct Radiative Effect of Aerosols (DREA) includes both natural and anthropogenic.

The discussion about the aerosol direct radiative effect and its potential influence on the Earth's climate began in the late 60s and early 70s (McCormick and Ludwig, 1967; Charlson and Pilat, 1969; Atwater, 1970). At this time, it begins to gain interest that changes in the aerosols concentration could be related to changes in the climate and meteorology of the planet. Early aerosol forcing assessments were based mostly on model simulations (Braslau and Dave, 1973; Lacis and Hansen, 1974; Weare et al., 1974; Charlock and Sellers, 1980; Coakley Jr et al., 1983; Cess et al., 1985). During the late 1990s and early 2000s, the increasing number of observations from the establishment of ground-based networks, the development and improvement of satellite sensors, and the development of field experiments around the world allowed progress in observational research (Boucher and Tanré, 2000; Rajeev and Ramanathan, 2001; Loeb and Manalo-Smith, 2005; Christopher and Zhang, 2002; Patadia et al., 2008; García et al., 2012).

Since then and to date, the direct radiative effects of aerosols have been determined using a combination of aerosol properties (such as loading, size distribution, chemical composition, and age), surface properties (surface albedo), and geographical parameters (Latitude and Longitude) (Yu et al., 2006). In particular, the complex interaction between aerosols and radiation is usually described with three optical parameters: Aerosol Optical Depth (AOD), Single-Scattering Albedo (SSA), and the Phase Function. The AOD determines the total

extinction of a light beam interacting with aerosols and is a proxy of their amount. SSA is the ratio between the scattering coefficient to the extinction coefficient, indicating the degree of particle light absorption. The phase function represents the angular distribution of scattered radiation.

Despite the advances in numerical modeling and observations, there are still major differences between modeling and observational studies, with the latter tending to have greater reductions in radiation. Both methods are associated with large uncertainties because of the inaccuracy of basic parameters. SSA accounts for much of this uncertainty (Myhre, 2009; Loeb and Su, 2010). Loeb and Kato (2002) combined the global measurements over the ocean of Clouds and the Earth's Radiant Energy System (CERES) with the TRMM Visible Infrared Scanner (VIRS) high-resolution imager to estimate the daily average DREA, finding that aerosols have a cooling effect over the Tropics of - 4.6 $\pm$ 1 W/m^2. Loeb and Manalo-Smith (2005) also used global measurements over the ocean of CERES but with MODIS (Moderate Resolution Imaging Spectroradiometer) Terra to compute a net total-sky (clear and cloudy) DREA at the Top of the Atmosphere (TOA) of -2.0 Wm^{-2}. Patadia et al. (2008) computed the first TOA cloud-free DREA over global land areas using Multiangle Imaging SpectroRadiometer (MISR), MODIS and CERES, estimating a DREA of -5.1 $\pm$ 1.1 Wm^{-2}. Su et al. (2013) combined a Model for Atmospheric Transport and Chemistry (MATCH) with MODIS to compute DREA, they also used data from Goddard Chemistry Aerosol Radiation and Transport (GOCART) model, to separate between anthropogenic and natural aerosols, thus, dividing between DREA and DRFA. Matus et al. (2015) estimated a global annually averaged DREA to be 1.9 Wm^{-2}, using CloudSat. Lacagnina et al. (2017) used optical properties retrieved by the Polarization and Anisotropy of Reflectances for Atmospheric Sciences coupled with Observations from a Lidar (PARASOL), the Ozone Monitoring Instrument (OMI), MODIS, and the global aerosol model ECHAM5-HAM2 to estimate DREA, finding a DREA at TOA to be 4.6 $\pm$ 1.5 Wm^{-2} for cloud-free and 2.1 $\pm$ 0.7 Wm^{-2} for all-sky conditions.

This chapter starts by characterizing aerosols properties and their Spatio-temporal variations

in the Aburrá Valley and Colombia. We estimate Bottom of the Atmosphere (BOA) DREA in the Aburrá Valley using ground-based sensors, including an SMP Smart Pyranometer, and a particulate matter monitor (BAM-1020). We also evaluated optical properties and DREA derived by a sunphotometer from AERONET. This study computes DREA over Colombia, combining CERES and MODIS measurements. Finally, we investigate aerosols' influence in energy fluxes and the evolution of the boundary layer.

2.2. Geographical and Air Quality context

Aburrá valley (Figure **2-1**c) corresponds to the natural basin of Medellín's river. It is located in the Department of Antioquia (Figure **2-1**b), Colombia (Figure **2-1**a), over the Andean mountain range. It is one of the most densely populated valleys of Colombia, with nearly four million inhabitants living in an area of 1152 km^2. Aburrá valley comprises ten municipalities, in a significant urban agglomeration: The Metropolitan Area of the Aburrá Valley, in which Medellín is the capital city.

The valley is 64 km long, with altitudes around the valley (west and east mountains) that vary between 3100 m.a.s.l. (Padre Amaya Peak) and 1300 m.a.s.l. Its widest cross-section, from divide to divide, is about 18.2 km wide.

During the last years, the air quality problem in the Aburrá Valley, as well as in other regions of Colombia, has been increasing, becoming one of the leading environmental concerns of the country's political agendas. In the Aburrá valley, PM2.5 is the only critical atmospheric pollutant, in terms of the thresholds established by EPA (Environmental Protection Agency of the United States), due to the high sulfur content in the fossil fuels sold. During March 2016, PM2.5 reached a daily concentration of up to 118 $\mu g/m^3$, in the worst critical air quality episode recorded so far.

PM2.5 in the valley comes from local and external sources. Local sources are mainly from

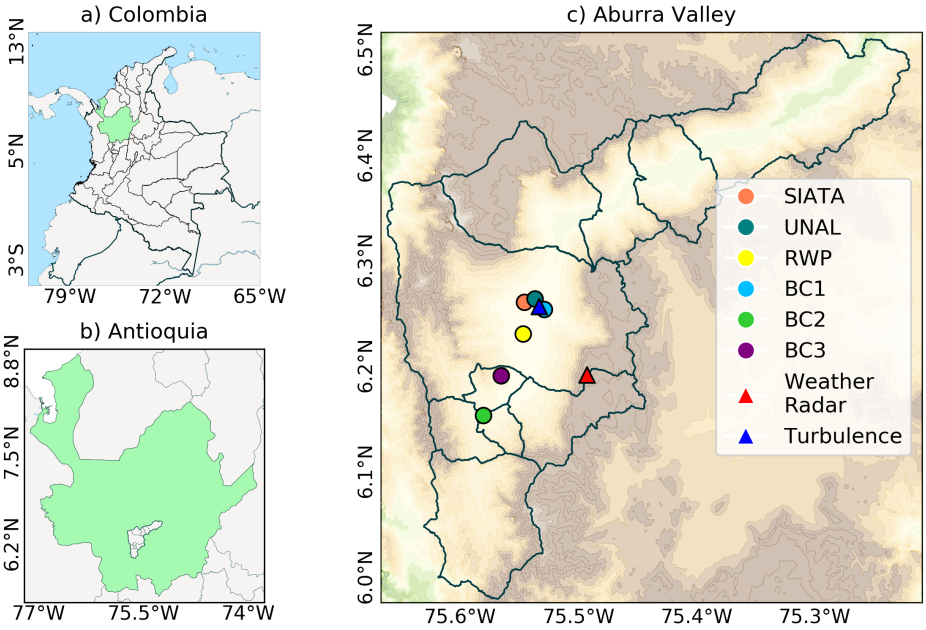

Figure 2-1: Geographical location of a) Colombia, b) The Department of Antioquia and, c) The Aburrá Valley. Panel (c) shows the SIATA's main operation centre (orange dot), where the pyranometer, the ceilometer, and the microwave radiometer are located; the teal dot shows the location of Universidad Nacional de Colombia (UNAL), where the sunphotometer and one PM2.5 station are located; the yellow dot indicates the location of the radar wind profiler used in this study; the blue, green, and purple dots indicate the location of the BC sensors; the red triangle correspond to the location of the weather radar; and the blue triangle corresponds to the turbulence sensor. The map (c) shows in colors from green to brown the main topographic features of the Aburrá valley.

mobile (80 %) and industrial (20 %) emissions (Universidad Pontificia Bolivariana and Área Metropolitana del Valle de Aburrá, 2017). However, other sources, such as the use of fireworks (Hoyos et al., 2020) and Biomass Burning (Mendez-Espinosa et al., 2019), can also have a significant influence on the air quality of the Aburrá Valley, and even over the entire Andean region.

Weather conditions in narrow valleys dominate the physical processes that promote or pre-

vent the accumulation of aerosols (Whiteman et al., 2014). In the valley, there are two very marked cycles for PM2.5: the diurnal cycle and the annual cycle. Regarding the annual cycle, the Aburrá Valley presents a maximum peak in PM2.5 concentration during February-March-April (FMA) (see Figure **2-2**a). This peak is a result of the combination of unfavorable weather conditions for vertical dispersion, local emissions, and aerosols coming from biomass burning to the north (The Caribbean Region) and west of Colombia (The Orinoquía region), as well as to the east of Venezuela.

Figure **2-2**a presents the annual cycle of PM2.5 in Medellín; Figure **2-2**b corresponds to the annual cycle of the number of fires to the north and to the east of Colombia. As it is shown, there is a significant similarity in both variables. Despite the great relationship, the number of fires cannot fully explain the high concentrations of PM2.5 during FMA in the valley. Weather conditions are also relevant. FMA corresponds to the transition period between dry and rainy conditions in the Andean zone. Stable conditions are almost permanent in this season due to a high presence of low-altitude clouds, limiting the amount of solar radiation and, therefore, the instability of the atmosphere.

The proximity of Colombia to the equator makes their incident solar radiation remains similar throughout the year. Despite this, its daily variations govern the diurnal cycle of lower-troposphere processes, which control the atmospheric stability and evolution of the Atmospheric Boundary Layer (ABL) (Yu et al., 2001; Whiteman et al., 2014). In the Aburrá valley, the diurnal cycle of particulate matter is modulated mainly by the diurnal cycle of the ABL height (see Figure **2-2**c-d) (Herrera-Mejía and Hoyos, 2019a). The ABL modifies the available control volume for the pollutants to interact and disperse (De Wekker and Kossmann, 2015; Lotteraner and Piringer, 2016).

To date, research has sought to determine the factors that modulate and dominate the air quality within the valley (Universidad Pontificia Bolivariana and Área Metropolitana del Valle de Aburrá, 2017; Herrera-Mejía and Hoyos, 2019a; Mendez-Espinosa et al., 2019; Hoyos et al., 2020; Roldán-Henao et al., 2020). However, this work aims to investigate the effects of

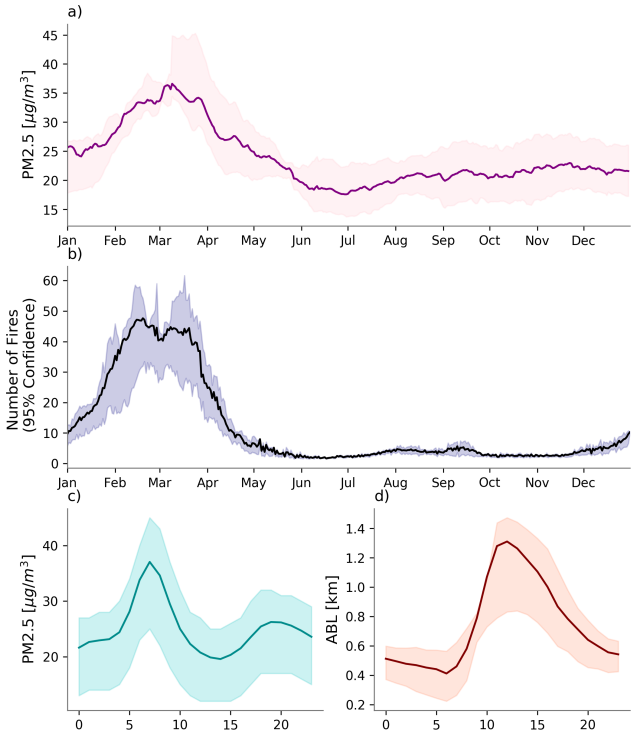

Figure 2-2: (a) Annual cycle of PM2.5 in the Aburrá valley, (b) Annual cycle of the number of fires in Colombia (source: MODIS Collection 6), (c) Diurnal cycle of PM2.5 in the Aburrá Valley, and (d) Diurnal cycle of ABL height in the Aburrá Valley. The shaded colors behind the line correspond to the 25 % and 75 % quartiles.

aerosols on local weather conditions. This first part focuses mainly on evaluating the optical properties of aerosols and the estimation of their effect on incident solar radiation.

2.3. Data

2.3.1. Local Network

- Air quality data

The metropolitan area of the Aburrá Valley has the largest PM2.5 monitoring network

in Colombia, with a total of 22 stations, operated by the local early warning system (Sistema de Alerta Temprana de Medellın y el Valle de Aburrá -SIATA-, www.siata.gov.co), a project of the local environmental authority: Area Metropolitana del Valle de Aburrá (AMVA). The PM2.5 equipment corresponds to eight Met One Instruments BAM-1020 and fourteen BAM-1022 monitors. This research uses hourly PM2.5 between March 2016 and January 2020 from four BAM-1020 located on the campus of Universidad Nacional de Colombia (UNAL), Medellín (see Figure **2-1**c), and in the points denoted as BC1, BC2, and BC3 in Figure **2-1**c. Three Magee Scientific AE33 Aethalometers are used for measuring aerosol Black Carbon (BC) every minute, based on a patented DualSpot TM technology and a multi-wavelength optical analysis. The AE33 aethalometers use seven optical wavelengths between 950 nm and 370 nm; in this research, We use the 880 nm wavelength. The illumination and analysis are performed at a 1-Hz time step.

- Aerosol optical properties

  Columnar aerosol optical properties in the Aburrá valley are also measured on the campus of Universidad Nacional de Colombia, Medellín (see Figure **2-1**c), using a sunphotometer integrated to the NASA Aerosol Robotic Network (AERONET) https://aeronet.gsfc.nasa.gov/. This instrument has operated since September 2012 (with missing data), providing AOD in eight different spectral bands (340, 380, 440, 500, 675, 870, 1020, and 1640 nm). In this study, we used AERONET level 1.5 data due to the limited observations satisfying level 2.0 (only 6 points recorded so far in the inversion product). We used both direct (AOD, fine/coarse mode AOD) and inversion products version 3 (SSA, Size Distribution, Absorption Optical Depth - AAOD -, and Radiative Forcing) between January 2012 and March 2020.

- Pyranometer

  The information of incident solar radiation between March 2016 and January 2020 was obtained from an SMP11 smart pyranometer located in SIATA main operation center

(Figure **2-1**c), on the roof of a 60-meter-high building. This instrument is a high-quality radiometer designed for measuring shortwave irradiance (270 to 3000 nm) on a plane surface (radiant flux, W/m^2), which results from the sum of the direct solar radiation and the diffuse sky radiation incident from the hemisphere above the instrument.

- Ceilometer

  We used cloud height retrievals from a Vaisala CL51 ceilometer (910-nm wavelength), in the same location as the SMP11. Ceilometers measure laser-pulse energy that is backscattered by clouds and other atmospheric components expressed as the backscattering attenuated coefficient (Emeis et al., 2012; Münkel and Roininen, 2010). The laser emits pulses every 67 ns, providing backscattering attenuated coefficient measurements with a vertical resolution of 10 m and temporal resolution of 16 s.

- Radar wind profiler

  Vertical wind profiles (RWP) are obtained every 5 minutes from a RAPTOR VAD-BL Doppler, located at the center of the valley (see Figure **2-1**c). This instrument relies on refractive index variations, caused by changes in humidity, temperature, and pressure. The Aburrá Valley RWP measures the wind profile in two different modes: a higher-resolution mode (60 m) that measures the wind profile from 77 to 3.500 m, and a lower-resolution mode (72 m) from 2.500 to 8.000 m. This study uses the former because ABL height never exceeded 3.500 m.

- Microwave radiometer

  We used a Radiometrics MP-3000A portable profiling microwave radiometer (MWR) to obtained Temperature and humidity profiles. These measurements are continually corrected in SIATA using radiosondes and multiple linear regressions. The MWR is located at SIATA's main operation center. The vertical resolution of the sensor is variable, depending on the atmospheric layer: 50-m resolution from the surface to 500

m, 100-m resolution from 500 m to 2 km, and 250-m resolution from 2 km to 10 km. For the aims of this study, we use the MWR profiles from March 2016 and January 2020.

- Turbulence Sensor (IRGASON)

  In this study, turbulent surface fluxes were obtained using an IRGASON, a sensor that applies the eddy-covariance theory. This sensor corresponds to an in situ, open-path, mid-infrared absorption analyzer integrated with a three-dimensional sonic anemometer. The gas analyzer can determine the absolute densities of carbon dioxide and water vapor, and the sonic anemometer measures orthogonal wind components at 20 Hz. Here we computed Latent (LE) and Sensible (H) Heat Fluxes, as well as the Turbulent Kinetic Energy (TKE) following:

$$H = \rho_a C_{pa} \overline{T'w'} \tag{2-1}$$

$$LE = L\rho_a \overline{w'q'} \tag{2-2}$$

$$TKE = \frac{1}{2}\left(\overline{(u')^2} + \overline{(v')^2} + \overline{(w')^2}\right) \tag{2-3}$$

  Where ρ_a is the density of the air, C_{pa} the heat capacity at constant pressure, T' the virtual temperature fluctuations, q' the fluctuations in H_2O (mixing ratio), L the latent heat of vaporization, and the overbar represents time averaging. The fluctuations in the wind velocity components are represented by u', v', and w'.

2.3.2. External Network

Satellite measurements provide information for regional- to global-scale assessments. The Terra spacecraft was launched on 18 December 1999 in a circular sun-synchronous polar orbit. It carries five instruments intended to monitor Earth's state of the environment. The Clouds and the Earth's Radiant Energy System (CERES) instrument is a scanning broadband radiometer that measures filtered radiances in the shortwave (0.3 and 5 μm), total (0.3

and 200 μm), and infrared window (8 and 12 μm). One CERES instrument operates in a cross-track scan mode to optimize spatial sampling for time-space averaging (Young et al., 1998), and the other in a biaxial scan mode that provides angular flux information that has improved the accuracy of angular models.

This research uses Terra edition 4.1 Single-Scanner Footprint TOA/Surface Fluxes and Clouds (SSF) 1-degree hourly (SSF1deg-Hour) product from 27 September 2007 to 05 February 2019. As Loeb et al. (2003) described in detail, the CERES SSF product combines radiances and fluxes with cloud and aerosol properties from coinciding high spatial and spectral resolution of the Moderate Resolution Imaging Spectroradiometer (MODIS) measurements. Aerosol optical properties in CERES SSF1deg-Hour product correspond to the total AOD at 0.55 μm and to the ratio of Optical Depth of Small Mode vs AOD from MODIS.

Despite the information provided by CERES on the aerosol properties, its spatial resolution is insufficient to characterize aerosols within the Aburrá Valley. Given this, the MODIS 6.1 Terra / Aqua 3km product is used for the period between January 2009 and August 2019. The MODIS 3 km Aerosol Product provides information on the AOD, aerosol size distribution, mass concentration, look-up-table-derived reflected and transmitted fluxes, and quality assurance (QA). This research uses the QA-filtered Scientific Data Set (SDS) known as Optical_Depth_Land_And_Ocean; this SDS contains only AOD values for the filtered, quantitatively useful retrievals over dark targets (Levy et al., 2013).

2.4. Aerosol Optical Properties in Colombia and the Aburrá Valley

Different aerosol types are associated with different sources and emission mechanisms, therefore exhibiting significant variations in optical properties (Dubovik et al., 2002). In this

section, we describe aerosol properties in Colombia and the Aburrá Valley, including size-dependent (i.e., the fine and coarse fractions) aerosol optical properties of the different types (scattering and absorbing aerosols). Fine Scattering AOD (FSAOD), Coarse Scattering AOD (CSAOD), Fine Absorbing AOD (FAAOD), and Coarse Absorbing AOD (CAAOD) are obtained using the Spectral De-Convolution Algorithm (SDA) Retrievals - Fine and Coarse Mode AOD from AERONET. Scattering AOD (SAOD) and absorbing AOD (AAOD) are estimated using SSA values, following:

$$SAOD_\lambda = (1 - SSA_\lambda) * AOD_\lambda \tag{2-4}$$

$$AAOD_\lambda = SSA_\lambda * AOD_\lambda \tag{2-5}$$

where λ correspond to the wavelength. Distinguishing between absorbing and scattering aerosols is essential to study the radiative effects of aerosols, and their potential impacts within the ABL. Both the backscattering and the absorption reduce the solar radiation reaching the surface; however, their consequent perturbations in the surface energy change with the aerosol type. Figure **2-3**a-b represents the percentage of the total AOD (440 nm) that comes from scattering (SAOD) and absorbing (AAOD) aerosols in the Aburrá Valley. As is seen, scattering aerosols are the most frequent type, embodying 86 % of the total AOD; its fine fraction contains the highest percentage with 71 % of the total. Since the sunphotometer measures only during clear-sky conditions, we decided to use the BC/PM2.5 ratio as another indicator of the absorbing percentage of the total aerosol. Figure **2-4**a shows the relation between SSA and BC/PM2.5 at the BC station closest to the sunphotometer (BC1, see Figure **2-1**c). There is a negative linear relationship between the variables, with a correlation coefficient of -0.61. Figure **2-4**b shows the BC/PM2.5 ratio at three different locations (BC1, BC2, BC3), as seen the absorbing percentage varies between 20.1 % and 28.7 %. Both SSA and BC/PM2.5 analyses indicate that aerosols in the Aburrá Valley are mostly scattering aerosols; however, the amount of absorbing aerosols is significant and could have important radiative effects within the ABL.

There are multiple sources of absorbing aerosols in the Valley; the most relevant include: 1)

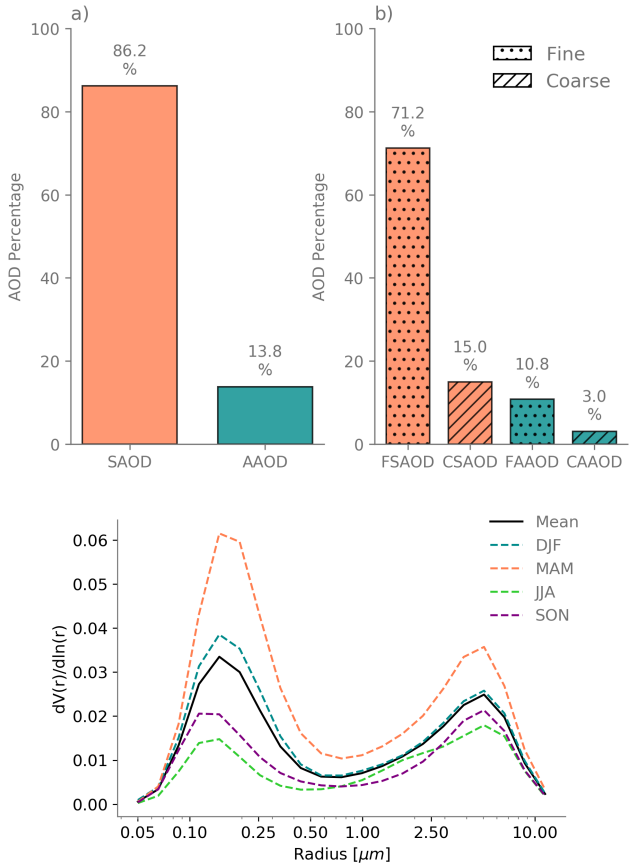

Figure 2-3: (a) Percentage of the total AOD that comes from scattering (SAOD, in orange) and absorbing (AAOD, in green) aerosols in the Aburrá Valley. (b) Percentage of the total AOD that comes from fine scattering (FSAOD), coarse scattering (CSAOD), fine absorbing (FAAOD), and coarse absorbing (CAAOD). c) Particle volume size distribution for different seasons in the Aburrá Valley.

the carbon content in the fossil fuel, and 2) the contribution of carbonaceous aerosols from biomass burning transport. According to Shi et al. (2019), the volume fraction of BC declined with aerosol aging, in biomass burning events. The monthly variations of BC/PM2.5 ratio indicate that the absorbing percentage decreases with increasing number of fires in Colombia (see Figures **2-4**c). However, this result does not mean that the BC content is lower, it is just that PM2.5 concentration is so high that this ratio becomes smaller. The diurnal variation of the of BC/PM2.5 ratio (Figure **2-4**d) show that the absorbing percentage increases during the rush hours. Notwithstanding, differences in relative humidity and ambient temperature,

fire intensity, the degree of aging of the particles, and the moisture content of the fuel (Reid and Hobbs, 1998; Jacobson, 2001), may be related to differences in absorption.

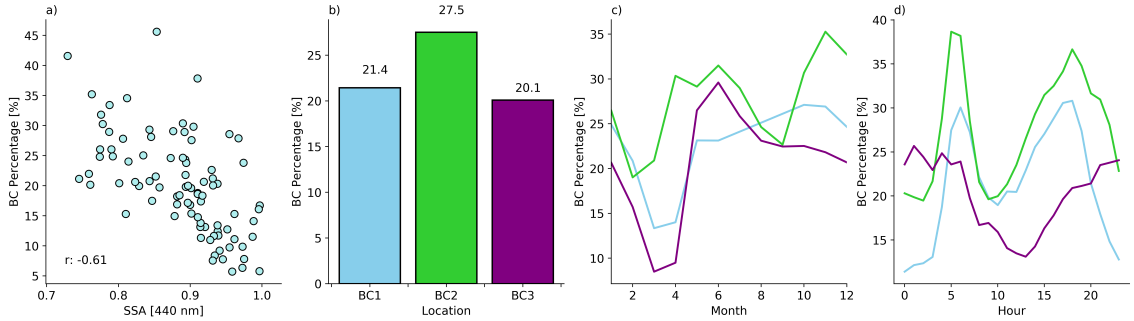

Figure 2-4: Particle volume size distribution for different seasons in the Aburrá Valley.

A comparison of the particle volume size distribution for different seasons in the Aburrá valley is presented in Figure **2-3**c. As noted by the mean curve (black line), the fine particle mode is higher than the coarse mode. Despite this, it is evident how this proportion is affected mainly by the significant increase in fine particle mode during MAM. For JJA and SON, the ratio between fine and coarse modes is equivalent. Particulate matter from biomass burning travels long distances (Freitas et al., 2005; Holanda et al., 2020) before arriving into the Aburrá Valley, and only the finest particles remain in the atmosphere during the travel. As shown in Figure1-2b during February-March-April, the number of fires increases significantly in Colombia; this can be the reason why MAM has the most considerable number of fine particles.

The wavelength dependence of AOD, commonly referred to as the Angstrom exponent (α), is an aerosol property used as an indicator of particle size. It is inversely related to the average size of the particles: the smaller the particles, the larger the exponent. Values greater than 2 indicate small particles associated with combustion byproducts, and values less than 1 indicate large particles (Schuster et al., 2006). A classification study over Aburra Valley is done using Gobbi et al. 2007 methodology. This method uses the Angström exponent curvature ($\delta\alpha/\delta\lambda$), computed as the difference between α values ($\delta\alpha$) measured in different wavelength ranges ($\delta\alpha = \alpha(440, 675) - \alpha(675, 870)$). Kaufman (1993) demonstrated that negative values of the $\delta\alpha$ indicate the dominance of fine-mode aerosols, while positive differences indicate

the effect of two separate particle modes.

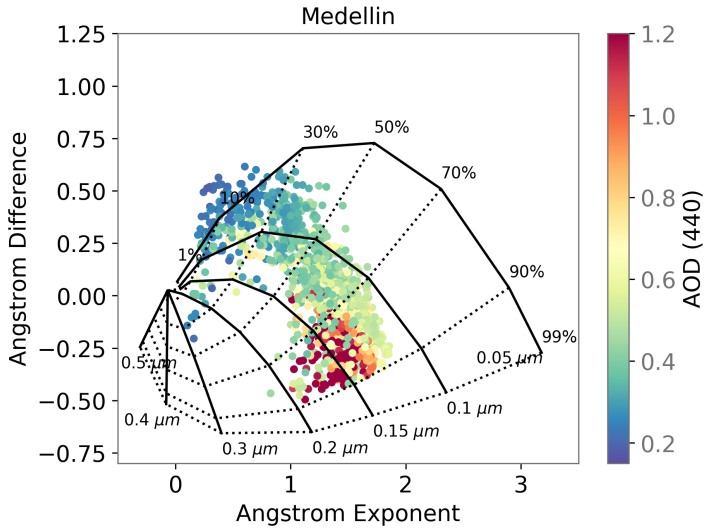

Figure 2-5: Angström exponent difference, $\delta\alpha = \alpha$(440–675 nm)– α(675–870 nm), as a function of α(440–870 nm) and aerosol optical depth (AOD) in color over Medellín. The black solid lines are each for a fixed size of the fine mode Rf and the dashed lines for a fixed fraction contribution of the fine mode to the AOD at 440 nm (η).

Figure **2-5** presents the Angström exponent difference as a function of α(440–870 nm) and aerosol optical depth (AOD). In this scheme the values of the AOD at 440 nm are represented using a color scale, the solid black lines indicate the fine-mode effective radius (Rf), and dotted lines indicate the contribution (η) (%) of the fine fraction to the total AOD. Data cluster around negative values of $\delta\alpha$ and large values of α ($2.2 > \alpha > 1$) indicate the dominance of fine-mode aerosols. As Figure **2-5** shows, while the optical depth increases, Rf also increases, going from an Rf of 0.05 to 0.15 μm. This significant increase in AOD and Rf could be linked with the aging process of aerosols, which affects the size distribution directly because of the coagulation and condensation process. However, it could also be related to the transport of particles from biomass burning in other regions of Colombia. Low AOD values (< 0.3) have lower Rf values, which evidences fine particles. Notwithstanding, much of this data is above ($\eta > 30$), which represents an important presence of coarse particles.

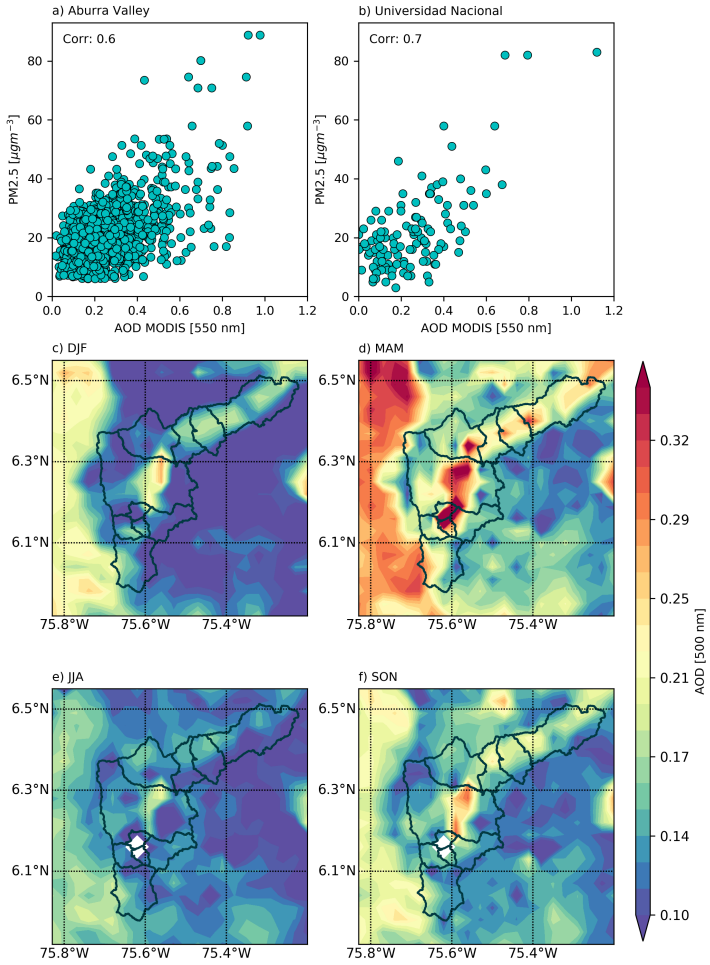

Figure 2-6: Relationship between AOD and PM2.5 in the (a) Aburrá Valley and (b) Universidad Nacional. c-f) Aerosol optical depth seasons variation in the Aburrá valley for the period between 2009-2019.

The spatial patterns of aerosols in the Aburrá Valley are analyzed using AOD (550 nm) from MODIS at 3 km. Figure **2-6**a-b shows the comparison of PM2.5 and MODIS AOD over the valley and at the campus of Universidad Nacional de Colombia. There is a linear relationship between both variables, with a correlation coefficient of 0.6 and 0.7, respectively. This result suggests that MODIS is congruent with ground-based measurements, and then, it is a good indicator of air quality near the surface. The intra-seasonal variations of AOD in the Aburrá valley are shown in Figures **2-6**c-f. It is evident the influence of urban emissions on aerosols concentration, since the largest AOD values locate in the center of the valley. This area is

where the greatest number of industrial activities and vehicle movements occur throughout the day. Therefore, particle concentration on the lowest part of the valley is higher compared to its hills.

During MAM in the Aburrá Valley, the transition season between dry and wet conditions favours atmospheric stability, inhibiting vertical dispersion of pollutants, and hence aerosol accumulation increases. Additionally, the transported aerosols from biomass burning intensify the concentration of PM2.5 significantly. The combination of these two mechanisms explain the annual cycle of aerosols in the valley, and therefore, AOD during this period is the highest, as expected. As seen from Figure **2-6**d, this increase is especially evident at the central and western parts of the valley, which strengthens the hypothesis that the leading processes do not only respond to the local but to the regional scale.

Aerosols in Colombia also have a very marked annual cycle. Figure **2-7** presents AOD retrieved from MODIS at different seasons. As in the Aburrá Valley, AOD during MAM reaches its maximum (Figure **2-7**a-d). High aerosol concentrations near the east of Colombia, Venezuela, and the Caribean are related to biomass burning for agricultural expansion. The historical fire frequency is presented in Figure **2-8**. The relationship between the number of fires and AOD in Colombia is evident. These fires are carried out in advance of the rainy season, which peaks in April. In this way, the low soil moisture favours the propagation of fires, and prepare the harvest for the rainy season. Aerosols in Colombia correspond mainly to small particles, as Figure **2-7**e-h shows with the Angström exponent. However, during MAM particles get even smaller throughout the national territory. As mentioned above, atmospheric particles emitted during biomass burning travel long distances, and only the smallest ones can remain in the air. That may be the possible reason for the result presented here. In DJF aerosols are especially finer in the southern part of the country, during JJA and SON in the eastern.

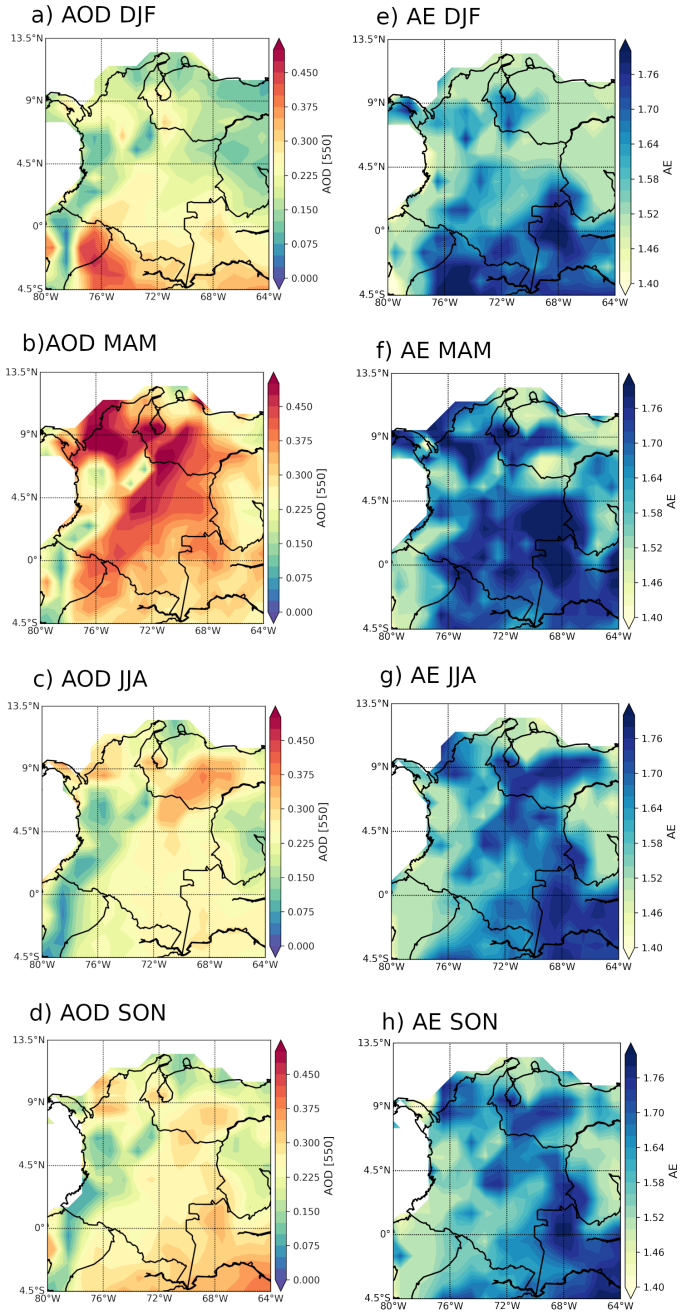

Figure 2-7: a-d) Seasonal variations of aerosol optical depth in Colombia for the period between 2009-2019. e-h) Seasonal variations of Angstrom exponent in Colombia for the period between 2009-2019

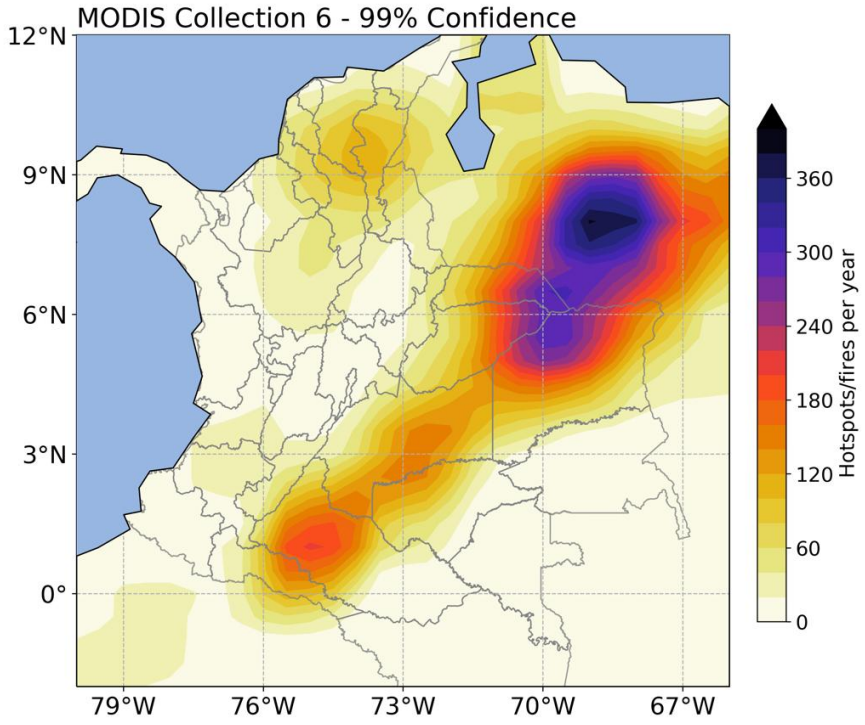

Figure 2-8: Historical fire frequency in Colombia.

2.5. Radiative effects of aerosols in the Aburrá Valley

DREA for a given location at latitude (θ) and longitude (ϕ) is commonly computed as the differences between radiative fluxes in the absence and presence of aerosols, as:

$$DREA(\theta,\phi) = \frac{1}{N_t}\sum_{t=1}^{N_t}[F_{sw}^{na}(\theta,\phi,t) - F_{sw}^{clr}(\theta,\phi,t)] \tag{2-6}$$

where $F_{sw}^{clr}(\theta,\phi,t)$ corresponds to the SW flux in the absence of aerosols for a specific time interval, and $F_{sw}^{na}(\theta,\phi,t)$ is the corresponding SW flux in the presence of aerosols. One of the main problems in solving this equation is finding a value for $F_{sw}^{clr}(\theta,\phi,t)$, since aerosols are always present in the atmosphere, even at low concentrations. For this reason, we implemented two different methodologies.

The first methodology corresponds to a statistical assessment for estimating the difference

in radiation for cases conditioned to high and low PM2.5 levels. Differences in radiation were computed within the diurnal cycle between 6:00 am and noon LT, and without clouds. Afternoon hours were not considered here because of the high cloud presence at these hours. To do this, we started filtering radiation with two different methods to eliminate the annual cycle: the fast Fourier transform and calculating the seasonal cycle, and removed it (i.e., calculated the anomalies). Subsequently, we selected clear-sky days by using cloud height derived from the ceilometer. We considered a day as cloudy when the number of hours with clouds presence between 6 am - 12 pm was higher than four. After selecting clear-sky days, we masked hours with clouds to minimize the error in the calculations. Finally, we defined high PM2.5 concentration using the 50th percentile of the distribution for each hour of the day. Values under the 50th percentile were considered *clean*, and values above the 50th percentile were labeled as *polluted*.

To assessing statistical significance in difference estimations, the nonparametric Wilcoxon–Mann–Whitney test (Mann and Whitney, 1947; DePuy et al., 2014) is used. This test evaluates whether any the two samples $X_1, X_2, ..., X_n$ and $Y_1, Y_2, ..., Y_m$ likely originate from the same distribution. Unlike parametric tests, the Wilcoxon–Mann–Whitney test does not assume normality or equal variance, and it uses the ranks of the data instead of their raw values. The null hypothesis states that the distributions of the populations $f[C(t)]$ and $g[C(t)]$ are identical. This test is calculated by the following:

$$U_n = nm + \frac{n(n+1)}{2} - R_n \tag{2-7}$$

$$U_m = nm + \frac{m(m+1)}{2} - R_m \tag{2-8}$$

where n is the sample size of $\{C(t)|WC\}$ (sample 1), m is the sample size of $\{C(t)|DC\}$ (sample 2), and R_n and R_m are the sum of the ranks in samples 1 and 2, respectively. R_n and R_m are obtained after ranking all the $n + m$ observations in a single sample $\{C(t)|WC\} \cup \{P(t)|DC\} = C(t)$. The normalized test statistic Z, which is approximately Gaussian for large samples, is defined as

$$Z = \frac{U - m_U}{\sigma_U} \tag{2-9}$$

where $m_U = nm/2$ and $\sigma_U = \sqrt{nm(n+m+1)/12}$. If $|Z|$ is greater than a predetermined cutoff value, then the null hypothesis can be rejected. We use 95 % significance as a threshold to reject the null hypothesis.

In the second methodology used, the zero aerosol flux was obtained as the radiation from models in surface and TOA. Radiation data modeled on the surface was obtained from the results of a theoretical radiation model for clear sky conditions implemented by Guzman (2018) in her master thesis. This model considers geometric relationships regarding the sun's incidence and the modification of that with the topography. Radiation modeled at the TOA was computed following the simple daily insolation formula:

$$Q_{day} = \frac{S_0}{\pi}\left(\frac{\overline{d}}{d}\right)^2 [h_0 sin\phi sin\delta + cos\phi cos\delta h_0] \tag{2-10}$$

where Q_{day} is the solar flux per unit surface area, $\overline{d}$ is the mean distance for which the flux density S_0 (i.e. the solar constant) is measured, d is the actual distance from the sun, δ corresponds to the declination angle, h is the hour angle, and ϕ is the latitude.

Figure **2-9**a-b shows the results for the statistical assessment for the cases where the annual cycle was eliminated using the FFT (a) and computing the anomalies (b). As can be seen, there are some differences between them. Still, their temporal variation and magnitude are very similar on average. The dotted gray line corresponds to the DREA, and the blue dots correspond to hours where the differences are statistically significant. The gray shadow corresponds to a sensible analysis of the PM2.5 threshold, varying between the 40th and 60th percentiles. In general, aerosols reduce the net solar radiation on the surface, and the higher reduction occurs in the early morning at 8:00 am LT.

Figure **2-9**c shows the result where the zero aerosol flux was taken as the modeled data by Guzman (2018), again the greatest DREA occur at 8:00 am; however, the magnitude of the difference present here is greater compared to the previous assessment. The main reason for this is because the statistical assessment underestimates the DREA. After all,

in the statistical assessment the values taken as zero aerosol flux still have some aerosol concentration. Figure **2-9**c shows the result where the zero aerosol flux was taken as the TOA modeled radiation. As can be seen, these reductions are very high, but they are mainly explained because of the attenuation of light as it travels through the atmospheric column.

The DREA of AERONET is present in Figure **2-9**e; as can be seen, we only show information until 10:00 am LT, this is because we do not have any inversion product of AERONET between 10:00 am and 2:00 pm. However, as it is shown, the higher reduction is again at 8:00 am. Compared to the two methodologies present before, the reduction computed with AERONET is higher. However, according to the previous studies as García et al. (2008), the AERONET network overestimated the DREA between 9 and 14 W/m2.

In general, the reduction in the surface net solar radiation increases with aerosol concentration. However, as shown in Figure **2-9**a, b, c, and e PM2.5 maximum, and DREA minimum do not coincide. As expected, the highest reduction happens when the radiation curve meets with the PM2.5 curve, because at this point, the available radiation is the greatest for the highest aerosol load. The interdependence of aerosol extinction on the Solar Zenith Angle (SZA) and the diurnal variation of aerosols amount (PM2.5 concentration) could explain the diurnal variation of DREA (Nemesure et al., 1995; Boucher et al., 1998; Yu et al., 2002).

Figure **2-9**f shows radiation during clear-sky conditions as a function of PM2.5 and SZA. There is an inverse linear relationship between these variables. Radiation reductions are evident for SZA lower than 70; for higher angles, the relationship is obscure.

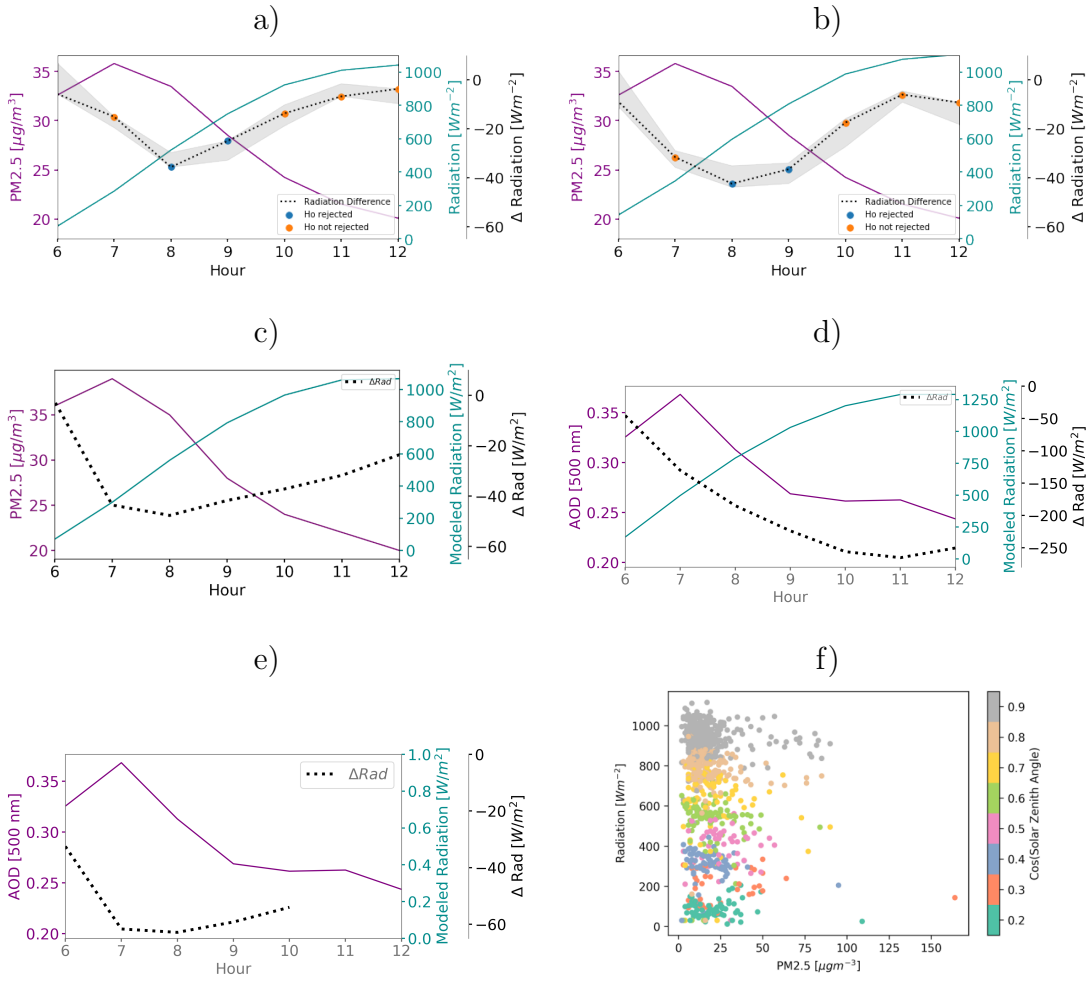

Figure 2-9: (a-b) Diurnal variations of the DREA (dashed line), Radiation with low aerosols (blue line), and the 50th percentile of PM2.5 concentrations (purple line), in a) radiation was filtered using the FFT and in b) using anomalies. (c-d) Diurnal variations of the DREA (dashed line) using modeled data in the c) surface as the zero aerosol flux and in the d) TOA. Blue and purple lines are the same as in (a-b). e) Diurnal variations of the DREA (dashed line) from AERONET.

The direct radiative effect from atmospheric aerosols is also investigated using the DREA values operationally provided in the AERONET webpage (http://aeronet. gsfc.nasa.gov). AERONET analyzes forcing at the Top Of the Atmosphere (TOA) in addition to the Bottom Of the Atmosphere (BOA), following:

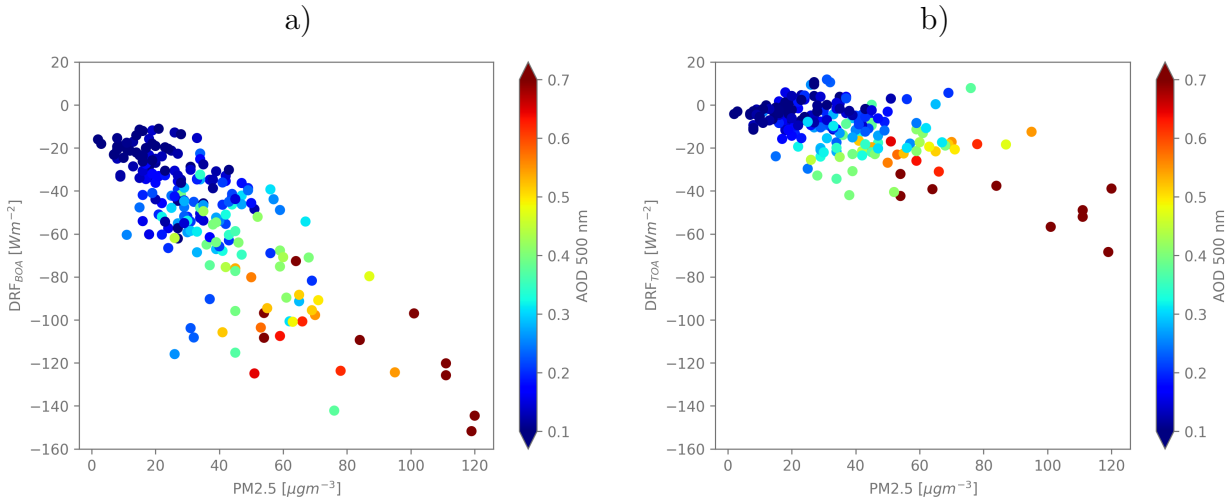

Figure 2-10: DREA provided by AERONET in the Aburrá Valley at (a) the BOT (surface), and (b) the TOP, as a function of aerosol concentration (PM2.5 - AOD).

$$\Delta FBOA_{AER} = (F_{BOA}^{\downarrow A} - F_{BOA}^{\downarrow C}) \tag{2-11}$$

$$\Delta FTOP_{AER} = (F_{TOA}^{\uparrow A} - F_{TOA}^{\uparrow C}) \tag{2-12}$$

where the arrows indicate the direction of the global fluxes: $\downarrow$ = downward flux and $\uparrow$ = upward flux. ΔF represents DREA in their respective location. DREA at (a) the BOT (surface), and (b) the TOP are displayed as a function of hourly PM2.5 concentration and AOD in Figure **2-10**. The aerosol effect at the BOA can be as low as -160 Wm^{-2} for an hourly PM2.5 concentration of 120 μgm^{-3}. March 2016 critical air quality episode has been the only month where these values have been recorded in the Aburrá Valley. Most of the time, PM2.5 concentration oscillates around 20 and 30 μgm^{-3}. According to figure **2-10**a, differences associated with these PM2.5 load are around -40 to -50 Wm^{-2}, coinciding with estimates from the SMP11. Unlike the surface, DREA at the TOP quantifies the difference in outgoing radiation fluxes. As shown in the radiative effect at the TOA, aerosols cool the atmospheric column, as mentioned by García et al. (2012) for urban-industrial aerosols when the surface albedo is less than 0.3.

2.6. Radiative effects of aerosols in Colombia

In this section, we use an approach proposed by Loeb and Kato (2002) and Loeb and Manalo-Smith (2005) that merges MODIS and CERES to estimate TOA DREA under clear-sky conditions. One advantage of using CERES to determine the DREA is that the measurements are acquired over broad spectral intervals in the shortwave (SW) and terrestrial-infrared or longwave (LW) regions. Nevertheless, a limitation is the coarse spatial resolution of measurements (Loeb and Manalo-Smith, 2005). Today, CERES provides information for both TOA and surface. However, this study only determined changes in surface radiation.

In order to compute DREA over Colombia, we use equation 2-6. Radiation in the absence of aerosols $F_{sw}^{clr}(\theta, \phi, t)$ is inferred from the relationship between SW surface radiation and aerosol optical depth. As described by Loeb and Manalo-Smith (2005), SW radiation is plotted against aerosol optical depth for each 1 ° interval of SZA. As seen in Figure **2-11**, there is a clear linear relationship between these variables. Therefore a regression line is fit to the data. The intercept of these regressions is extrapolated to zero AOD. It approximates the mean "no aerosol flux" as a function of SZA. According to Loeb and Kato (2002) the uncertainty in $F_{sw}^{clr}(\theta, \phi, t)$ can be determined to within 1 Wm^{-2} in any given region. Loeb and Manalo-Smith (2005) also point out that the principal sources of error are uncertainties in CERES-derived fluxes, AOD retrievals, and changes in surface wind speed.

Figure **2-12** shows the DREA for the period between 2007 - 2019 of simultaneous CERES/MODIS observations. Regions of maximum aerosol direct radiative effect are evident over the northeast of Colombia, and Venezuela due to biomass burning. In these areas, DREA can be lesser than -40 Wm^{-2}. The less pronounced aerosol direct radiative effect in Colombia appears along the Andean mountain range, where AOD records are also low. (see Figure **2-12**). Both peaks are closely related to biomass burning, the first with burning mainly in eastern Colombia and Venezuela, and the second with burning in the Amazon basin.

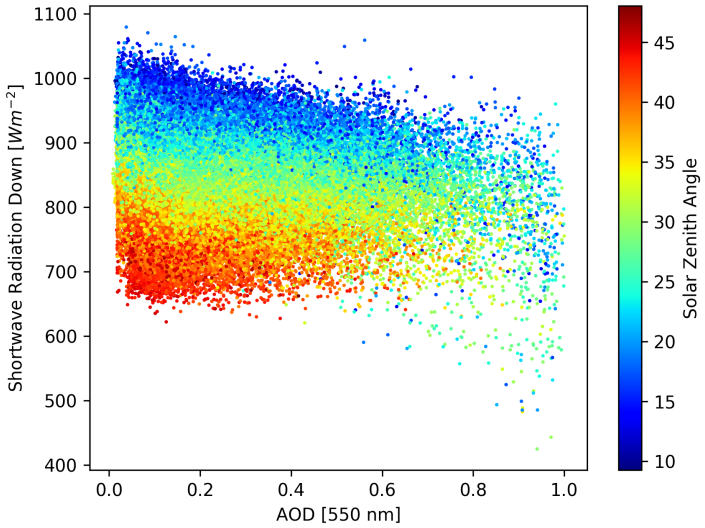

Figure 2-11: CERES shortwave radiation in Colombia as a function of MODIS AOD (550 nm) and Solar Zenith Angle during clear-sky conditions.

Although AOD is higher from February to April, DREA is maximum during August. The direct radiative effect of aerosols does not depend exclusively on the aerosol load but on aerosol load, aerosol composition, SZA, available radiation, among others. Figure **2-12** shows monthly variations of these variables in Colombia. Note that even though AOD is maximum in February - March - April (FMA), SZA and radiation available is lower compared to the months where the second peak of aerosols occurred. The average slope of the fitted lines for each SZA is shown in Figure **2-13**. The smaller the SZA, the more negative the slope, which would further explain why the differences are greater in the second half of the year than the first.

2.7. Perturbations in aerosol-radiation-ABL interactions

The ABL is directly influenced by and rapidly responds to the diurnal cycle of solar radiation; thus, any variation of the solar radiation reaching the surface will change the ABL evolution. Daytime solar radiation warms the surface, favouring thermal instability and tur-

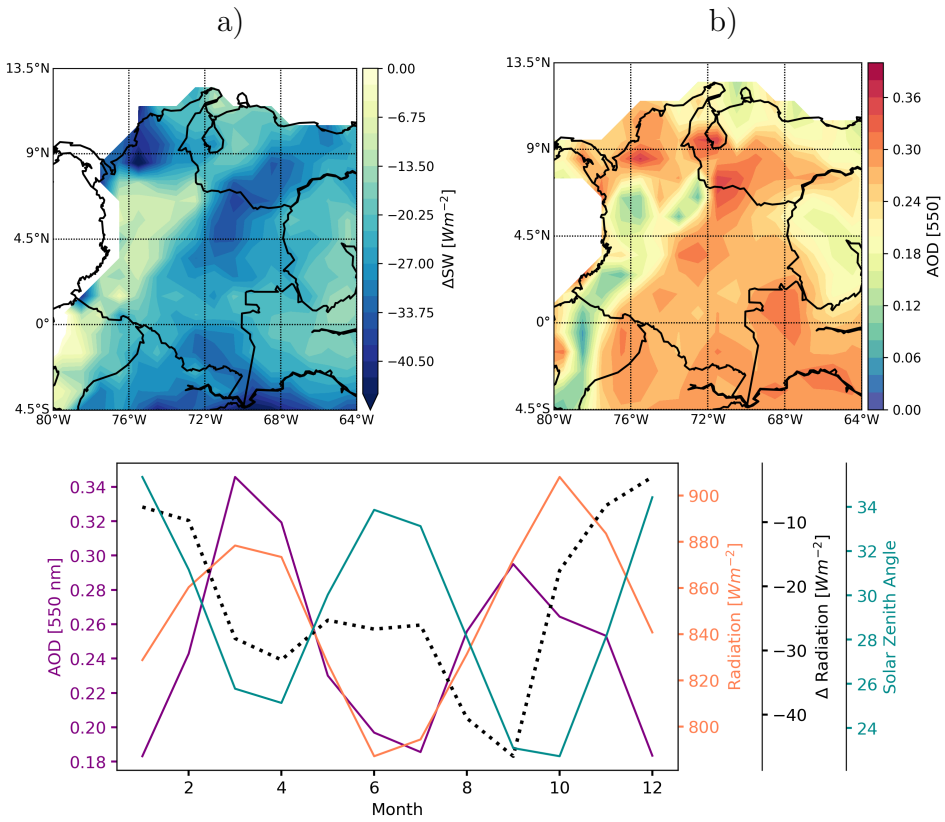

Figure 2-12: a) Direct radiative effect of aerosols based on clear-sky CERES SW radiation over Colombia and b) Average aerosol optical depth measured by MODIS over Colombia between 2017 - 2019. c) Monthly variation of the direct radiative effect (dashed black line), aerosol optical depth (purple line), shortwave radiation (orange line), and solar zenith angle (blue line).

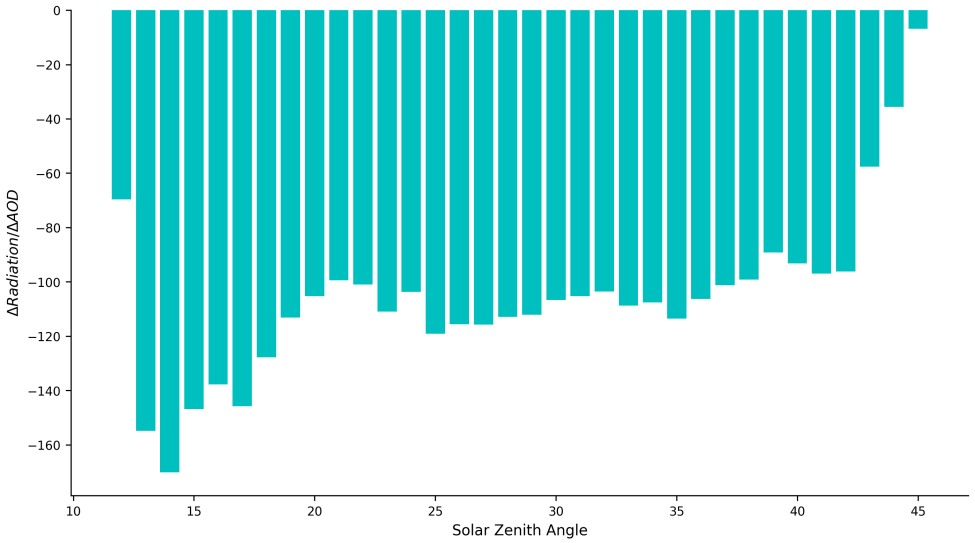

Figure 2-13: The average slope of the fitted lines for each solar zenith angle in Colombia.

bulent mixing. In the Aburrá Valley, during clear-skies days, the convective boundary layer can extend to a height of 1.5 – 2 km or more (see Figure **2-14**). Intense turbulent mixing homogenizes its conserved properties, like, potential temperature, specific humidity, and atmospheric pollutants like aerosols (Yu et al., 2002). In this section, the ABL height is used to investigate aerosol-radiation-ABL interactions. We used the ABL height estimations obtained by (Herrera-Mejía and Hoyos, 2019b), using a Richardson number-based methodology (Stull, 1988; Chandra et al., 2014; Zhang et al., 2014) that combines microwave radiometry information with radar wind profiler information.

The ABL interacts directly with aerosols, altering the radiative fluxes by scattering and absorption of solar radiation (Coakley Jr et al., 1983; Charlson and Pilat, 1969; Penner et al., 1994; Yu et al., 2002; Li et al., 2017). As mentioned before, aerosols in the Aburrá Valley largely reduce the incident solar flux absorbed by the surface. The reduction in the surface solar radiation by aerosols leads to a significant ABL perturbation. Figure **2-14**a shows the diurnal changes in the height of the ABL for clear-skies days in the Aburrá Valley. As shown, on average aerosols in the Valley lowers the top of the ABL by as much as 300 meters. The reduction in the ABL Height occur for all aerosol types. Figure **2-13**b-c) shows the relation between ABL Height and Absorbing AOD nm and Scattering AOD at 440,

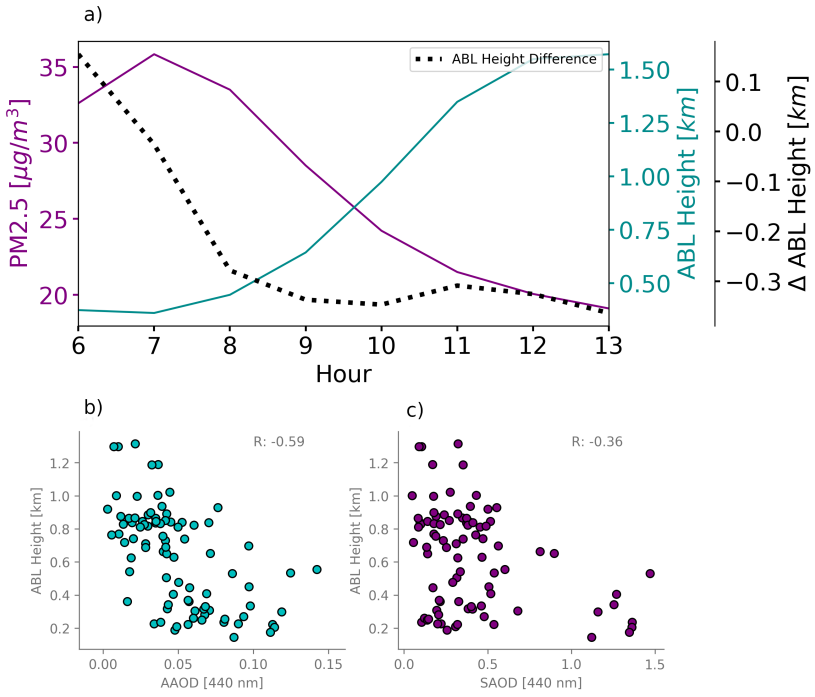

Figure 2-14: a) Diurnal differences on the ABL Height between a pristine and a hazy atmosphere (dashed line) between 0600 LT and 1300 LT, ABL Height with low aerosol concentration (blue line), and the 50th percentile of PM2.5 concentrations (purple line). b) Relation between ABL Height and Absorbing AOD at 440 nm, c) the same as (b) for Scattering AOD.

respectively. As observed, there is an inverse linear relationship for both aerosol fractions; however, the correlation coefficient is higher for AAOD (-0.59). This result implies that the greatest perturbations within the ABL will occur when the atmospheric emissions have a significant content of BC.

According to Yu et al. (2002), aerosols exert pronounced impacts on the energy fluxes and evolution of the ABL depending on the aerosol single-scattering albedo, purely scattering aerosol lowers the top of the ABL, and strongly absorbing aerosol raises it. Generally, aerosols cool the surface and lower atmosphere by the reduction of shortwave, sensible heat, and latent heat fluxes. Absorbing aerosols induce atmospheric heating; therefore, they do not naturally

feedback to lower ABL Height. In this situation, the lower ABL Height may be caused by the reduction of sensible heat at the surface (Li et al., 2017).

To investigate the diabatic heating due to absorbing and scattering aerosols, we used thermodynamics profiles to compute the Dry-diabatic and Diabatic heating profiles in the Aburrá Valley, following:

$$MSE = C_pT + gz + L_vr \tag{2-13}$$

where MSE corresponds to the Moist Static Energy, C_p is the specific heat at constant pressure for air, T is the absolute temperature, g is the gravity acceleration, z is the height at a given reference level, and r is the vapor mixing ratio. MSE corresponds to a thermodynamic variable, analogous to equivalent potential temperature. Details are presented in (Wallace and Hobbs, 2006). Diabatic heating is the rate of change of MSE per unit time ($d(MSE)/dt$).

Figure **2-15** shows the Dry-Diabatic Heating anomaly and the Diabatic Heating anomaly profiles conditioned to the 75th and 25th quantile of SSA. As can be seen, when SSA is equal to or less than its 25th quantile (i.e. very absorbing aerosols), the atmospheric column heats up by as much as 0.4 $kj/kgDay$ for the Dry-Diabatic Heating case and 0.2 $kj/kgDay$ for the Diabatic Heating case. Heating induced by absorbing aerosols is especially important below two km., within the ABL. Unlike absorbing aerosols above the ABL, absorbing aerosols within the ABL may not stabilize the boundary-layer inversion cap since there is strong vertical mixing in the ABL due to aerosol-induced atmospheric heating. The heating profiles for scattering aerosols are, on the other hand, very close to zero. This result was as expected since these aerosols are the most common in the Valley, representing 85 % of the total aerosol fraction.

We can say that maybe other factors such as water vapor or aerosol concentration could be the reason for these differences. Figure **2-16**a shows the same analysis as Figure **2-15** for relative humidity; as you can see, the difference in relative humidity between the scattering and absorbing aerosols is almost equal to zero below 2 km. Hence they cannot explain the

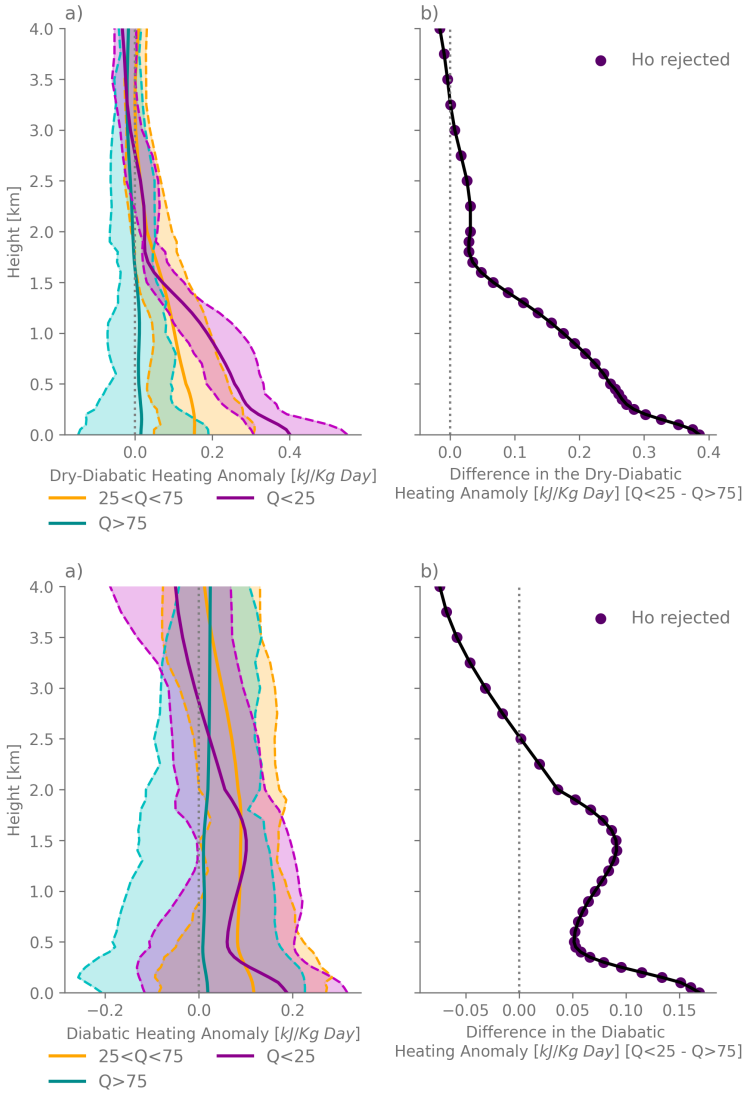

Figure 2-15: a) Dry-Diabatic Heating anomaly profiles conditioned to the 75th (Q75) and 25th (Q25) quantile of SSA in the Aburrá Valley. b) Difference in the Dry-Diabatic Heating anomaly profiles. c-d) same as (a-b) for the Diabatic Heating anomaly.

differences in the heating profiles. In addition, Figure **2-16**c corresponds to the distribution of PM2.5 concentration for both absorbing and scattering aerosols. As seen, the distribution is also very similar, and hence this couldn't be the reason either. Finally, remember that the sunphotometer measures only during clear sky conditions. Hence, these profiles do not show all the thermodynamic profiles distribution; they are only showing the part when we have clear sky conditions.

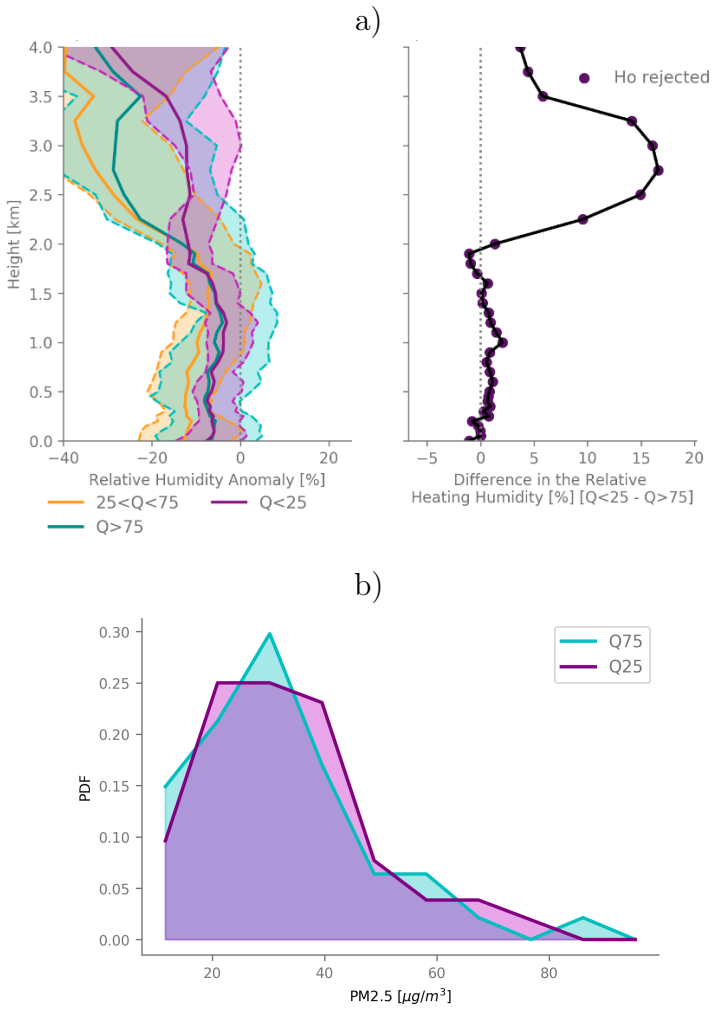

Figure 2-16: a) Relative humidity anomaly profiles conditioned to the 75th (Q75) and 25th (Q25) quantile of SSA in the Aburrá Valley. b) Probability density function for PM2.5 concentration conditioned to the 75th (Q75) and 25th (Q25) quantile of SSA in the Aburrá Valley.

Despite absorbing aerosols warms up the atmospheric column, both scattering and absorbing aerosols reduce surface energy fluxes. Figure **2-17** presents the diurnal cycle of the sensible heat flux, the latent heat flux, and ABL Height in different scenarios. Due to the limited period of turbulent energy fluxes measurements (three months), this analysis includes the data under all-skies conditions. In this particular case, absorbing and scattering aerosols were classified using the BC/PM2.5 ratio described before. We divided the days with mainly absorbing and mainly scattering aerosols using the 25th and 75th quantiles of the BC/PM2.5 ratio. In this sense, days with ratios higher than the 75th quantile were classified as absorbing, and days with ratios lower than the 25th quantile were classified as scattering.

The presence of both scattering and absorbing aerosols reduce the amount of solar radiation reaching the surface, then both sensible and heat fluxes decrease in the presence of aerosols. Even knowing that absorbing aerosols warm up the atmospheric column, sensible heat flux decreases because this variable does not depend on the magnitude of the temperature but on the gradient between the skin and atmospheric temperature. When we increase atmospheric temperature because of absorbing aerosols, this gradient also decreases, and hence sensible heat flux.

As shown in Figure **2-17**a-b) changes in the sensible and latent heat fluxes are especially important when aerosols are mainly absorbing (Q75 BC/PM2.5), and particularly between 1000 LT and 1500 LT. For absorbing aerosols, the sensible heat flux also has significant differences after 1500 LT. Generally, when aerosols are mainly scattering, differences are less pronounced.

Turbulent Kinetic Energy (TKE) is one of the most important variables in micrometeorology, because it measures the intensity of turbulence. It is linked to the momentum, heat, and moisture transport through the boundary layer. As in sensible and latent heat fluxes, TKE decreases in aerosols' presence, especially for absorbing aerosols, as shown in Figure **2-17**c). This reduction in the TKE could also explain the ABL variations.

Atmospheric aerosols affect the surface buoyancy flux and the capping inversion, both of

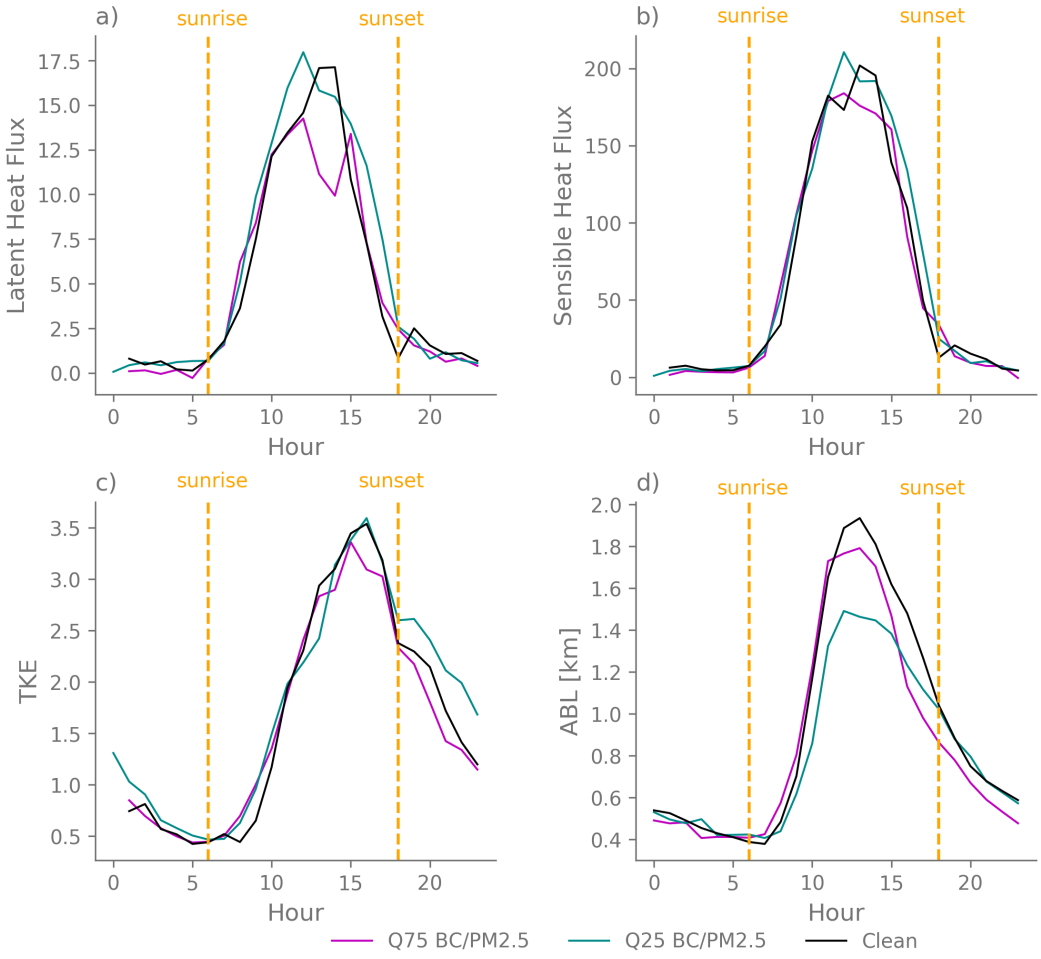

Figure 2-17: Diurnal cycle of a) Latent heat flux during clean atmospheres (clean), atmospheres with the presence of mainly absorbing aerosols (Q75 BC/PM2.5, magenta line) and atmospheres with the presence of mainly scattering aerosols (Q25 BC/PM2.5, blue line), b-c-d) the same as (a) but for Sensible heat flux, Turbulent Kinetic Energy, and ABL Height, respectively.

which determinate the diurnal changes in the ABL Height. As shown in Figure **2-17**d, aerosols inhibit the growth of the top of the ABL, especially when aerosols are mainly scattering, which could be related to the significant reduction in solar radiation, and the subsequent cooling of the atmospheric column. In contrast, absorbing aerosols reduce the solar radiation in the surface, but they also warm up the atmospheric column. Thus, as mention before they do not naturally feedback to lower ABL Height.

This result suggests the existence of positive feedback between aerosols and ABL. The greater the aerosol concentration, the less solar radiation on the surface, thus reducing energy fluxes and therefore reducing the ABL height and causing it to collapse earlier. This inhibition of the ABL Height favors an increase in aerosols concentration near the surface, resulting in the feedback. However, given the limited number of data and the fact that we have all-sky conditions, this result is not robust enough yet.

2.8. Final remarks

Most aerosols in the Aburrá Valley are particles with a diameter of less than 1 micrometre with a high content of black carbon (between 20 % and 28 %). During February-March-April, Colombia has its largest fire season, which affects air quality both in its entire territory and in the main cities of the country. The occurrence of fires, as well as the usual dynamics of cities, lead to a significant increase in PM2.5 concentration in Medellín and its Aburrá valley, which can alter the climate and meteorology of the city.

Nowadays, aerosols are one of the primary atmospheric pollutants in Colombia and the Aburrá Valley. They can alter radiative and energy fluxes near the surface through scattering and absorption of solar radiation, thus affecting the evolution of the ABL. This study investigates the radiative effects of aerosols in Colombia and the Aburrá valley, using a vast combination of ground-based sensors and satellite information.

The presence of aerosols in the Aburra Valley act to decrease solar radiation on the surface. Diurnal variations of these reductions show a major peak ($\sim$ -40 Wm^{-2}) in the early morning at 0800 LT when there is high aerosol load and also enough solar radiation. During air pollution episodes direct radiative effect of aerosols can be as significant as -160 Wm^{-2} in just one hour. Colombia also presents significant reductions in solar radiation due to the presence of aerosols. Biomass burning triggers most of these reductions. Thus, the most significant reductions in Colombia are in the Caribean and Orinoquía regions ($\sim$ -45 Wm^{-2}), places with the highest frequency of fires in the year.

The reduction in solar radiation also leads to a decrease in sensible and latent heat fluxes, which could induce important feedbacks. The presence of aerosols inhibits the growth of the ABL height by almost 300 meters, especially when aerosols are mainly scattering. Absorbing aerosols within the ABL warm up the atmospheric column; therefore, they do not naturally act to suppress ABL Height. This reduction in ABL Height and its subsequent early collapse could result in a positive feedback between aerosols and ABL, in which aerosols reduce the ABL Height and this reduction favors aerosols accumulation near the surface.

3 Aerosol Indirect Effect Assessment over Colombia and the Aburrá Valley Using Ground-based and Satellite Information

3.1. Introduction

Cloud-aerosol interactions remain one of the primary sources of uncertainty in the Earth's energy budget estimation (Boucher et al., 2013). Aerosols can directly affect the climate system through scattering and absorption of solar radiation, and indirectly serving as Cloud Condensation Nuclei (CCN) and Ice Nuclei (IN). In 1974 Twomey suggested that increasing the atmospheric aerosols concentration will result in more CCN, more cloud droplets with smaller sizes, and consequently, increase the solar radiation reflected by clouds. This hypothesis applies to clouds with the same liquid water content. Since then, numerous observational and modelling studies have evaluated this hypothesis in different scenarios and cloud regimes (Pawlowska and Brenguier, 2000; Nakajima et al., 2001; Bréon et al., 2002; Garrett et al., 2004; Quaas et al., 2008; Kleinman et al., 2012; Werner et al., 2014; Christensen et al., 2016; Jia et al., 2019). Among the most famous observational evidence of the aerosol effect in clouds are ship tracks, which became widely recognized with the emergence

and advancement of remote sensing from space (Coakley et al., 1987; Radke et al., 1989). As ships travel across the ocean, sulfate particles in their exhaust produce more cloud drops that are smaller in size, and therefore forming brighter clouds.

Additionally, because all clouds droplets must form on preexisting CCN, this aerosol indirect effect, in turn, determines to a large extent the precipitation-forming processes (Rosenfeld et al., 2008). According to Albrecht (1989), the increasing number of CCN suppresses precipitation and results in brighter clouds. However, multiple studies have shown positive and negative feedbacks between aerosols and precipitation, evidencing the system's complexity. For instance, in shallow clouds, submicrometer aerosols decrease precipitation (Radke et al., 1989; Rosenfeld, 2000, 1999; Rosenfeld et al., 2006; Andreae et al., 2004) and invigorate deep convective rain clouds with a warm ($\geq 15°C$) cloud base (Molinié and Pontikis, 1995; Bell et al., 2008; Fan et al., 2018).

As discussed in Rosenfeld et al. (2008) and in Altaratz et al. (2014), aerosols, clouds and precipitation interactions occur in multiple ways. The radiative effects of aerosols on clouds mostly act to suppress precipitation, since they reduce the amount of solar irradiance reaching the land surface, and hence cause less heat to be available for evaporating water and energizing convective rain clouds (Ramanathan et al., 2001). Absorbing aerosols such as Black Carbon (BC), heat the air above the surface. This heating stabilizes the lower atmosphere and limits the formation of convective clouds (Koren et al., 2004). The surface cooling generated in the presence of bright aerosols can also alter the atmospheric circulation system.

Even though the physics of the Twomey effect are well established and described on the particle scale (micrometres) (Twomey et al., 1974), how this relationship is expressed at a large scale (hundreds of kilometres) remains uncertain. Several atmospheric models suggest diverse magnitudes of the Twomey effect (Feingold et al., 1994; Tao et al., 2012). Consequently, increasing the observational data to quantify and constraint the effect is needed. Additionally, given that previous studies have presented contrasting results depending on their location or the cloud types, assessing the Twomey effect (1974) and the Albrecth (1989) effect under

different scenarios and cloud regimes is desirable.

This study corresponds to an evaluation of the aerosols indirect effect, starting from the aerosol-cloud-precipitation interactions in the regional (over Colombia) and local (over the Aburrá Valley) scales. For this aim, we use aerosol optical properties and cloud properties from the Moderate Resolution Imaging Spectroradiometer (MODIS) Collection 6.1. Since MODIS does not simultaneously measure aerosols and cloud properties, we determine to some extent the concentration of aerosols in cloud formation using the nearest pixel to the cloud, using a 1-degree grid. We also use ground-based sensors to measure thermodynamics profiles and precipitation.

This chapter is organized as follows: Section 2.2 includes the geographical context of the Aburrá Valley and Colombia. Section 2.3 introduces the variables and datasets used. Section 2.4 presents a characterization of clouds in the Aburrá Valley, using MODIS information, section 2.5 examinates Cloud Effective Radius (CER) variation as a function of height, monthly variations, and Cloud Water Path (CWP) in the Aburrá Valley. Section 2.6 assess aerosol-precipitation interaction using ground-based sensors. Section 2.7 evaluates the Twomey effect in Colombia with MODIS data at 1x1 degree resolution. Finally, section 2.8 presents the main conclusions of this study and establishes future work recommendations.

3.2. Geographical context

Colombia is a country located in the north of South America, bounded on the north by the Caribbean Sea, and the west by the Pacific Ocean. The geography of Colombia is delineated by six main natural regions that present their unique characteristics. These regions are the Andes mountain range, the Pacific coast, the Caribbean coast, the Llanos (plains), the Amazon Rainforest, and the insular area, which comprised islands in both the Atlantic and Pacific oceans.

Colombia, located within the tropics, exhibits climate variations within the six natural regions and depends on the altitude, temperature, humidity, winds and rainfall. Climate zones in Colombia include tropical rainforests, savannas, steppes, deserts and mountain climate. Figure **2-1**a presents the geographical location of Colombia.

In recent years, the increasing number of illegal forest fires associated with agricultural expansion, have been deteriorating air quality conditions in Colombian territory. As a result, some of the main cities in Colombia, such as Bogota, Medellín and Bucaramanga, have reported days of unhealthy air quality conditions associated with the transport of biomass burning emissions. Additionally, the constant anthropogenic emissions in cities and the unfavourable meteorological conditions for pollutant dispersion have led to the occurrence of critical air quality episodes in large cities.

In recent years, the city of Medellín, along with its metropolitan area, has experienced several critical air quality episodes during February-March-April. These episodes have made visible the urgency of measuring and understanding the dynamics of air quality in the territory, as well as quantifying their possible impacts. Hence, Area Metropolitana del Valle de Aburrá (AMVA), the environmental authority in Medellín, decided to implement an extensive network for monitoring air quality and other meteorological variables in the local territory.

Medellín and its metropolitan area are located in the Aburrá Valley, which in turn is located in the department of Antioquia, as shown in Figure **2-1**. Aburrá Valley is the natural basin of the Medellín's River and its located over the central Andean mountain range. The valley is 64 km long, with altitudes around the valley (west and east mountains) that vary between 3100 m a.s.l. (Padre Amaya Peak) and 1300 m a.s.l. Its widest cross-section, from divide to divide, is approximately 18.2 km wide, and in its narrowest section the valley is about 3 km wide.

Air quality records from the last decade have shown that only PM2.5 is a critical pollutant in the study region, being the only pollutant that exceeds unhealthy air quality standards

according to the United States Environmental Protection Agency (EPA). Previous studies have mentioned the role of both the meteorology (Herrera-Mejía and Hoyos, 2019a; Roldán-Henao et al., 2020) and the transport of biomass burning aerosols (Mendez-Espinosa et al., 2019), in the modulation and detonation of critical air quality episodes.

3.3. Data and Methodology

In previous studies, the Twomey effect has been evaluated in terms of Cloud Droplet Effective Radius (CER, r_e) (Hansen and Travis, 1974), which is a weighted mean of the size distribution of cloud droplets. This variable is operationally retrieved from remote-sensing observations, given that CER is closely related to light-scattering properties of clouds (Nakajima and King, 1990). However, CER is a function of the Cloud Water Path (CWP) and the Cloud Droplet Number Concentration (Nd), therefore, it is necessary to constraint the problem for constant CWP. Given that, it is preferable to use Nd instead of CER when evaluating cloud-aerosol interactions. Nd can be computed from Cloud Optical Thickness (COT, τ_c) and CER following:

$$N_{\mathrm{d}} = \frac{\sqrt{5}}{2\pi k}\left(\frac{f_{\mathrm{ad}} c_{\mathrm{w}} \tau_{\mathrm{c}}}{Q_{\mathrm{ext}} \rho_{\mathrm{w}} r_{\mathrm{e}}^5}\right)^{1/2} \tag{3-1}$$

where Q_{ext} is the unitless extinction efficiency factor that is approximated by its asymptotic value of 2 (Hulst and van de Hulst, 1981), K is a parameter that links CER to the mean volume radius, f_{ad} is a constant values that varies between 0.1 and 0.9, ρ_w is the density of liquid water (1000 kgm^{-3}), and C_w is the rate of increase of CWP with height, and can be computed as follows:

$$c_{\mathrm{w}} = \rho_{\mathrm{a}} \frac{c_{\mathrm{p}}}{L_{\mathrm{v}}} \left(\Gamma_{\mathrm{m}}(T, P) - \Gamma_{\mathrm{d}}\right) \tag{3-2}$$

where ρ_{a} is the parcel air density, $c_{\mathrm{p}} = 1004\ JKg^{-1}K^{-1}$ is the specific heat of dry air at constant pressure, L_v is the latent heat of vaporization, and $\Gamma_{\mathrm{d}} = -g/Cp$ ($\mathrm{g} = 9.81\ ms^{-1}$) and

Γ_m are the dry and moist temperature lapse rates, respectively. Further details are present in Grosvenor et al. (2018). When assuming adiabaticity conditions, the above equations can be express as:

$$N_d = \gamma \tau_c^{\frac{1}{2}} r_e^{-\frac{5}{2}} \tag{3-3}$$

with $\gamma = 1.3 \cdot 10^{-}5\ \mathrm{m}^{-0,5}$ (Quaas et al., 2008).

3.3.1. Regional Scale

The Moderate Resolution Imaging Spectroradiometer (MODIS) is an instrument aboard Terra and Aqua satellites, that travel around the globe measuring properties of both clouds and aerosols, as well as other environmental variables. The MODIS aerosol product measures the ambient Aerosol Optical Deep (AOD) globally at 550 nm. The cloud product determines both physical and radiative cloud properties, using a combination of infrared and visible techniques. In this section, we use daily Level 3 data from Terra retrievals at 1-degree grid between 12 °S and 18 °N and 60 °W and 85 °W, and between January 2012 and December 2019. The MODIS Level 3 products include cloud properties divided by the thermodynamic phase (ice/water) (King et al., 2003; Platnick et al., 2003), and aerosol optical depth (AOD) at 550 nm.

To evaluate the aerosol-cloud interaction in this region, we decided to compute Nd using equation 3-3. As Grosvenor et al. (2018) suggested, Nd estimations were obtained only when COT was higher than 5. MODIS can not measure aerosol and cloud properties simultaneously; however, the MODIS daily retrievals are averaged into a 1-degree grid that combines information on clouds and the surrounding aerosols (unless the grid box is completely clouded). The Probability Density Functions (PDF) for Nd in liquid and ice cloud droplets were compared with intervals of AOD. The same was done for CER and CWP. Finally, Nd variations as a result of AOD were evaluated in terms of the slope for Nd percentiles.

3.3.2. Local Scale

To assess cloud-aerosols interactions over the Aburrá Valley, we use MODIS Terra Level 2 products for both clouds (MOD06_L2) and aerosols (MOD04_3K). Since MOD06 and MOD04 have different spatial scales (1km and 3km, respectively), we reshape both datasets to a 0.03-degree grid. As in the regional section, we use aerosol and optical properties between January 2012 and December 2019. We limit our analysis to the region between 6 °N and 6.5 °N and 75.3 °W and 75.6 °W.

In the local scale, simultaneously AOD and cloud properties were computed as the spatial mean values of both variables in daily resolution. CER measurements as a function of AOD and CWP are present for different cloud types. In this section, we classify cloud types using a modified version of the methodology proposed by the International Satellite Cloud Climatology Project (ISCCP), in which Cloud Top Pressure (CTP) and COT measurements are combined to obtain nine basic categories (Rossow et al., 1985). Figure **3-1** shows the classification table.

Before analyzing the Twomey effect, we compared the ISCCP and MODIS measurements for the first half of 2017 in the Aburrá Valley (not shown). We found significant variations between both datasets. Despite the differences, we decided to continue with this methodology, because the final purpose of this classification is not to determine with certainty the cloud type but to separate clouds into similar sets. Additionally, the databases are never combined in the analyzes presented here.

Since CER changes with height, we decided to assess CER and CWP variations as Rosenfeld (1999) did for convective clouds. We analyze the relationship between CER and Cloud Top Temperature (CTT), but we included the nine cloud types. We also separate CER and CTT relationship at two-month intervals, so that the monthly variations could be determined. This assessment was also made for CWP. As Rosenfeld (1999) explained, a satellite image is a snapshot at an instant in time, so to infer the vertical time evolution of the individual

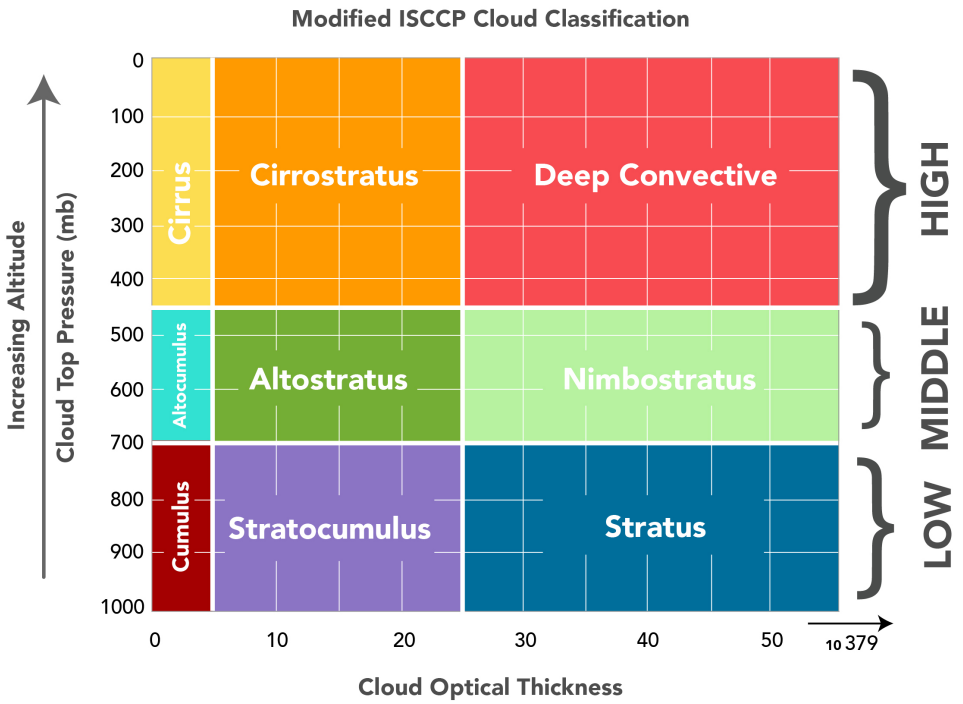

Figure 3-1: The modified version of the cloud classification table provided by the ISCCP

clouds, one must assume that properties observed simultaneously for cloud at different stages are similar to the properties of a single cloud as it grows (Arakawa and Schubert, 1974).

Aerosol-precipitation interaction in the Aburrá Valley was assessed using ground-based sensors. In this study, we utilised thermodynamic variables measured for the microwave radiometer described in chapter 2, section 2.2, and PM2.5 information measured with a BAM-1022 located in the campus of Universidad Nacional de Colombia (see Figure **2-1**).

Precipitation data were obtained using radar-based QPE estimations, based on a technique described in Sepúlveda (2015) and Sepúlveda and Hoyos (2017) using radar reflectivity fields, a disdrometer, and rain gauge information. The Aburrá valley weather radar consists of a 350-kW C-band polarimetric and Doppler radar manufactured by Enterprise Electronics Corporation and operated by SIATA. Given the radar scanning strategy, precipitation

information is obtained every five minutes with a spatial resolution of nearly 128 m. The uncertainty with the QPE is lower than 10 %.

The size distribution of precipitated hydrometeors in the valley was obtained with a disdrometer located in the SIATA main operation centre (Figure **2-1**c). This equipment measures the quantity, size and speed of the drops, and in this way estimates the equivalent reflectivity on the ground. All variables included in the aerosol-precipitation interaction assessment were retrieved between January 2014 and January 2020.

3.4. Cloud characterization in the Aburrá Valley

Topographic features highly condition cloud properties in the Aburrá Valley, as seen through Figure **3-2**a-f. The highest mountains of the Aburrá valley, that is, its eastern and western hills, have the biggest percentage of cloud cover, with approximately 55 %, compared to the central area of the valley, which ranges from 35 % to 40 % (see Figure **3-2**a). This difference of up to 20 % is due to the influence of the mountain range, which causes the air to rise. While the air rises, it cools, and at the dew point temperature, clouds form. Important cloud coverage is also present in the Samana Valley (to the southeast of the Aburrá Valley), which occurs mainly due to the high humidity and orography of the region.

According to MODIS measurements, around 1030 LT, the clouds over the Aburrá Valley are frequently Cirrus (around 39 % of the time) and Cirrostratus (around 33 % of the time), as seen in Figure **3-2**b. However, due to the limitations of satellite information, it is essential to clarify that there are a large number of low-altitude clouds over the valley that are not commonly recorded by these sensors. Despite, it is evident that clouds over the hills are optically thicker than clouds in the centre part, which is also seen in Figure **3-2**f. Therefore they could be associated with higher precipitation rates compared to the clouds in the centre of the valley.

Another important finding is that cloud droplets over the mountains are smaller to clouds in the centre part, with a difference of about 5 μm. As seen in Figure **3-3**b, CER is highly dependent on cloud-top temperature, which is strongly related to cloud height (the lower the temperature, the higher the cloud); therefore, colder clouds are associated with larger CER, especially when the temperature is lower than -40 $°C$. Figure **3-2**e shows average Cloud Top Temperature (CTT) over the Valley, as shown, clouds over and around the mountains are warmer compared to clouds in the centre, indicating that the clouds within the Valley are higher compared to the clouds in the mountains. These spatial differences in droplet size seem to be triggered mainly by cloud height, and not by CWP, as expected.

As mentioned before, mountains systems favour air rise and therefore clouds formation. Despite this, clouds in the centre of the Valley seem to be higher compared to clouds over the mountains. Two different hypotheses could explain this result; the first could be the fact that clouds in the centre were classified as cirrus (i.e. thin and high), and thus may not respond to local forcings, but regional forcings. The second is that these clouds are formed because of temperature gradients. Since the Aburrá Valley is located in the tropics near the equator, these temperature gradients are usually very large.

Since aerosols act as cloud condensation nuclei, they especially modified droplet sizes, as the Twomey effect theory explains. Figures **3-3**a-d assess the impact of CWP, CTT and COT in CER changes. CWP is one of the main variables that are known for its significant impact on CER. However, Figures **3-3**a and **3-3**d show that this relation is necessary but not sufficient, in a sense that there are not small droplets when CWP is high, but it can be small droplets for small CWP values. When we analyze CER as a function of CWP and COT (Figure **3-3**d), it is evident that an increasing linear relationship exists between CWP and CER for each COT interval. As seen, the standard deviation for this linear relationship increases with CER. Therefore, it is concluded that CER is especially sensitive to changes in water content when cloud droplets are smaller.

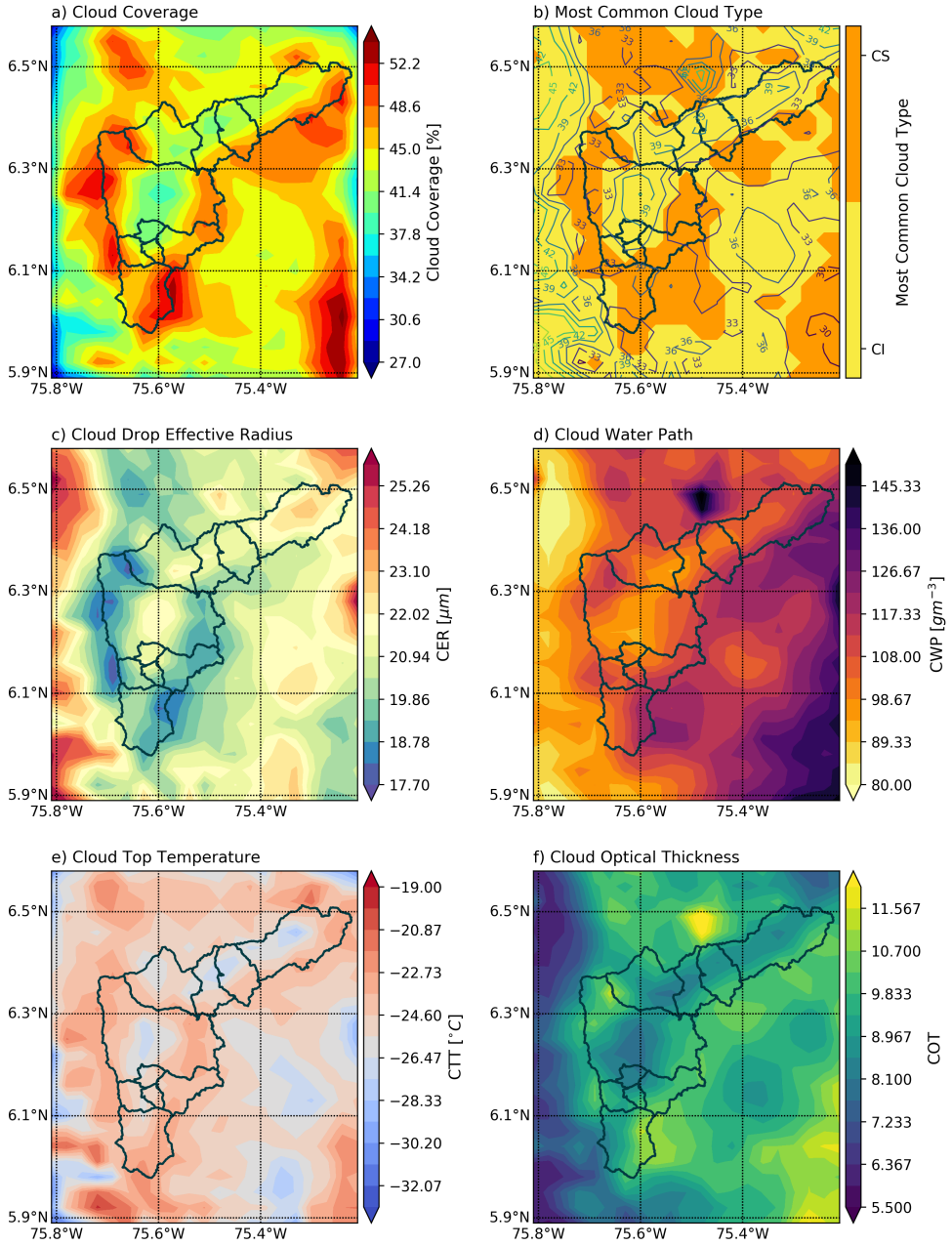

Figure 3-2: Cloud properties in the Aburrá Valley for the period between 2012 - 2020, using MODIS collection 6.1. a) Cloud coverage; b) Most common Cloud types in yellow (Cirrus) and orange (Cirrustratos). Contour lines correspond to the percentage of the particular cloud type to the total cloud coverage. c) Cloud Drop Effective Radius; d) Cloud Water Path; e) Cloud Top Temperature; f) Cloud Optical Thickness.

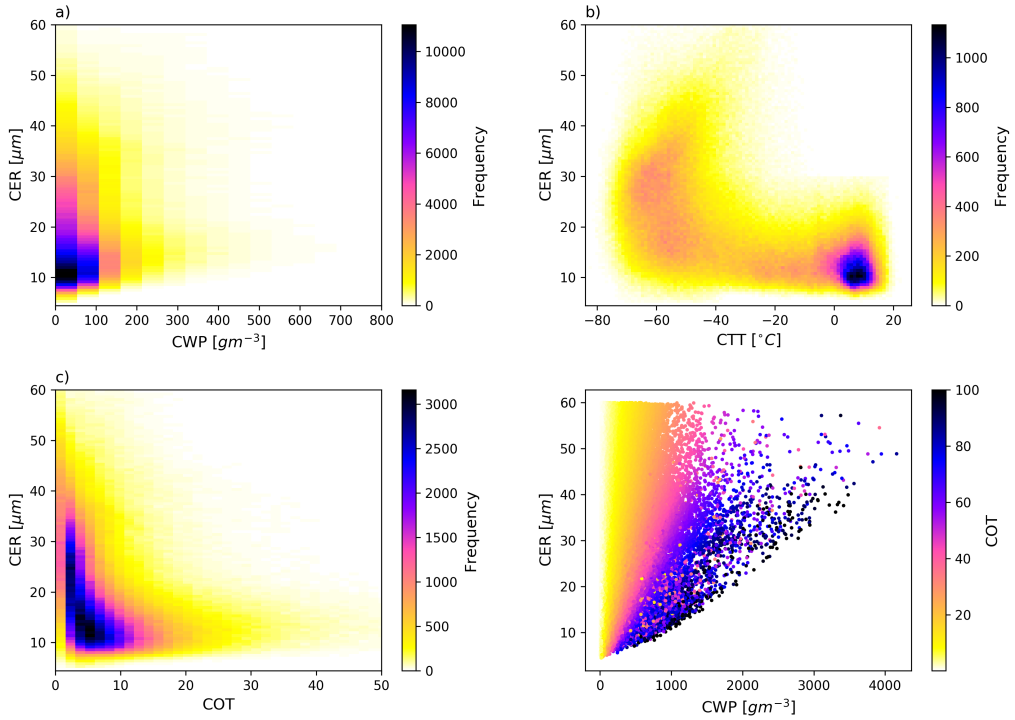

Figure 3-3: 2D histograms with the number of measurements for the relationship between a) CER and CWP, b) CER and CTT, c) CER and COT. d) CER as a function of CWP and COT.

As for the CWP, the relationship between the COT and the CER seems to be necessary but not sufficient. There are not big cloud droplets for large values of COT, but it is possible to have small cloud droplets for small values of COT. Mainly, CER seems to decrease with COT in an exponential function. Finally, as mention before CER tends to increase with the decrease of temperature (or increase in height).

To make a first approach to the interactions between aerosols and clouds, Figures **3-4** and **3-5** present the spatial distribution of cloud properties as in Figure **3-2**, but conditioned to cases when PM2.5 in the valley was lower than its 25th percentile (Figure **3-4**) and higher than its 75th percentile (Figure **3-5**).

As can be seen, the cloud coverage is almost the same for both cases, main differences are located outside the valley, in the Samana region, where the cloud coverage increase in more than 5 %. When aerosol concentration increases, the cloud drop effective radius are smaller inside and around the valley, as Figures **3-4**c and **3-5**c shows, this result is the first evidence of the Twomey effect in the study region. However, as indicated before, CER in the valley are highly dependent in the CTT or cloud height. Following this, Figures **3-4**e and **3-5**e shows that during hazy conditions, clouds tend to be warmer.

Koren et al. (2005) studied aerosol-cloud interaction in the Atlantic ocean; they used profiles of the relationship between cloud properties and aerosol and showed a reduction of the CER for higher AOD. They also showed that while the cloud optical depth of water clouds increases with AOD the cloud optical depth of ice clouds decreases, hence the total COT stays constant.

In the Aburrá Valley clouds and aerosols are both affected by changes in meteorological conditions, which vary mainly with the passage of the Intertropical Convergence Zone (ITCZ), that is, at the time of year. Therefore, it is not easy to associate the results found here solely to the aerosol increase. For this reason, in the next section, we decided to analyze the CER and CWP partitioned into different clouds types and months.

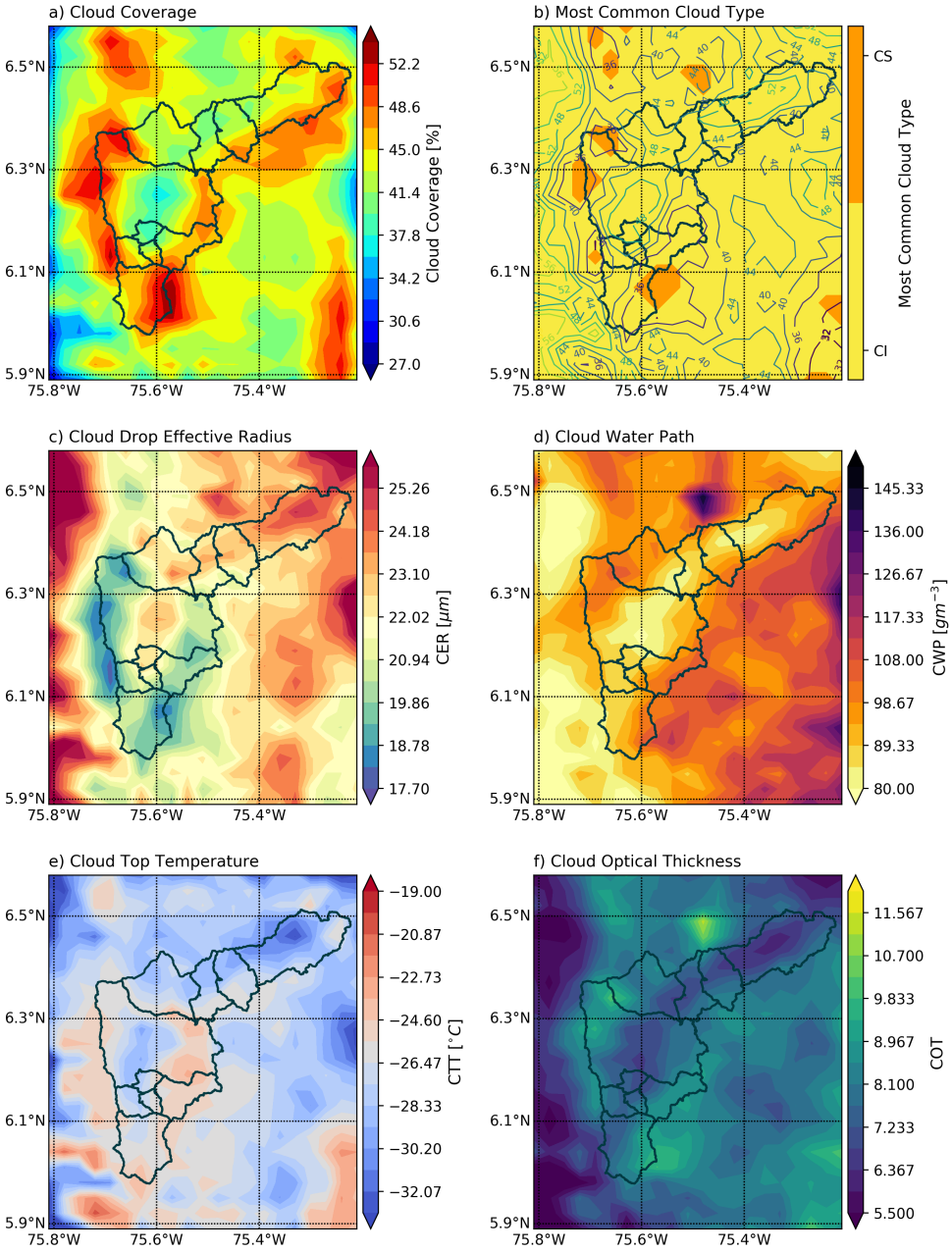

Figure 3-4: Cloud properties in the Aburrá Valley for the period between 2012 - 2020, using MODIS collection 6.1. a) Cloud coverage; b) Most common Cloud types in yellow (Cirrus) and orange (Cirrustratos). Contour lines correspond to the percentage of the particular cloud type to the total cloud coverage. c) Cloud Drop Effective Radius; d) Cloud Water Path; e) Cloud Top Temperature; f) Cloud Optical Thickness.

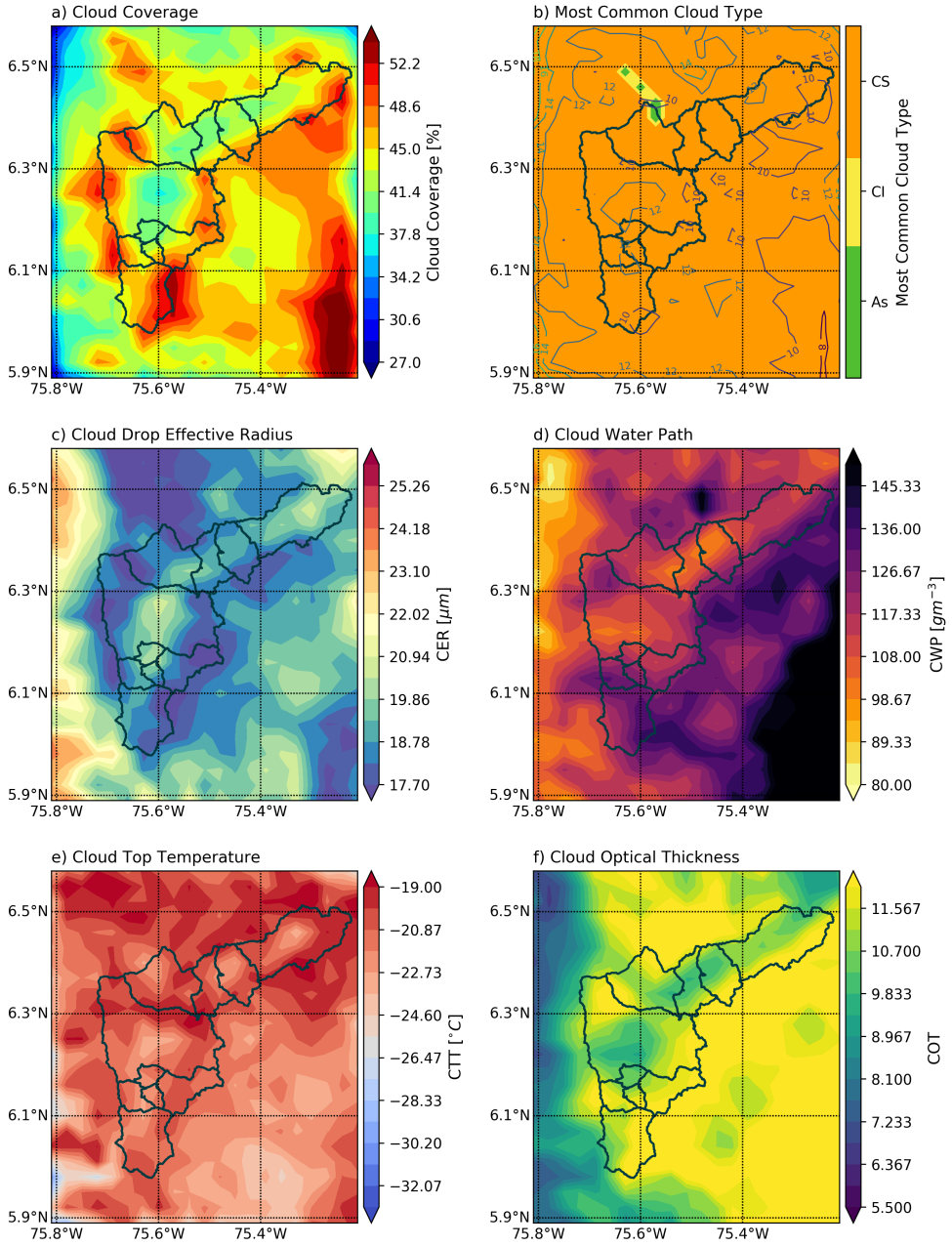

Figure 3-5: Cloud properties in the Aburrá Valley for the period between 2012 - 2020, using MODIS collection 6.1. a) Cloud coverage; b) Most common Cloud types in yellow (Cirrus) and orange (Cirrustratos). Contour lines correspond to the percentage of the particular cloud type to the total cloud coverage. c) Cloud Drop Effective Radius; d) Cloud Water Path; e) Cloud Top Temperature; f) Cloud Optical Thickness.

3.5. Aerosol-cloud interaction over the Aburrá Valley

According to Rosenfeld and Lensky (1998), the dependence of CER to CTT for growing convective clouds reveals the evolution of cloud droplets and hence the various processes leading to precipitation formation. They established the following five distinct zones from the evolution of convective clouds microstructure with temperature:

- **Diffusional droplet growth zone:** This is where rain processes have not significantly progressed. It is characterized by very slow CER growth with CTT, expressed by the shallow slope of d(CRE)/d(CTT).
- **Droplet coalescence growth zone:** This is where cloud drops grow by coalescence into raindrops. It is characterized by a rapid CER growth with CTT, expressed by a large slope of d(CRE)/d(CTT).
- **Rainout zone:** This is where the warm rain is fully developed. In this zone, CRE stays stable between 20 and 25 μm.
- **Mixed phase zone:** Here, there is an apparent additional increase of CRE, which is related to the development of the ice phase. It occurs at CTT $< 0°C$.
- **Glaciated zone:** This is when all cloud drops are glaciated. Here CRE reaches its maximum size because there is not an efficient mechanism for ice particles growth.

Here, we applied a modified version of Rosenfeld and Lensky (1998) methodology, using MODIS information. Figure **3-6** shows monthly variations of the relationship between CRE and CTT of convective clouds in the Aburrá Valley. It is evident how CER in Feb-Mar is smaller compared to the rest of the months. According to Rosenfeld et al. (2014), the diffusional droplet growth zone is where the effective radius is lower than a critical value ($r_e < r_{e,cri}$), where warm rain starts to develop. It has been shown that the critical radius is around 14 μm (Rosenfeld and Gutman, 1994).

As seen in Figure **3-6**, during Feb-Mar CER is lower to 14 μm until around -5 $°C$. However, at this point, CER continues growing very slow until around -25 $°C$, where it starts to grow faster. This slow growth of CER with temperature during Feb-Mar suggests that the diffusion process of cloud droplets in the Valley is retarded because of the high aerosol concentration. During the rest of the year, CER also grows very slow until around -5 $°C$, probably because Aburrá Valley corresponds to an urban area with a relatively high concentration of aerosols during the whole year. However, unlike Feb-Mar, cloud droplets start growing faster from -5 $°C$. In figure **3-6** is easy to identify the diffusional zone and maybe the mixed-phase zone. The coalescence zone is not present. Nevertheless, it is important to mention that for the different months, the atmosphere will be subject to a different large-scale forcing. Which will affect cloud development, such as subsidence, lifting, etc.

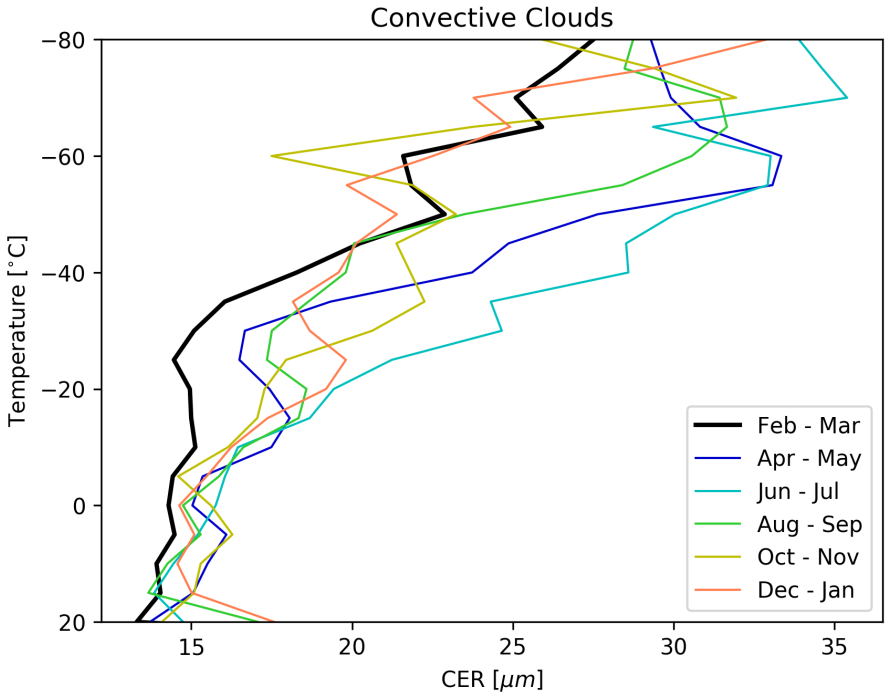

Figure 3-6: Monthly variation of the relationship between Cloud Top Temperature and Cloud Effective Radius, for the convective clouds in the Aburrá Valley. The solid black line represents February and March, which corresponds to the most polluted time in the Valley, as seen in Figure **2-2**

To study the aerosol effect in the rest of the cloud types defined by the ISCCP, we evaluated monthly variations of the relationship between CER and CTT in each cloud type, as shown in Figure **3-7**. Here, we aren't looking to distinguish cloud droplets' evolution rather to compare CER in different cloud regimes and months. As mention before, CER depends on multiple variables, such as cloud water content. Figure **3-8** shows the monthly variations of the relationship between CWP and CTT. Figure **3-7** and **3-8** were done to assess whether CRE changes relied on CWP changes.

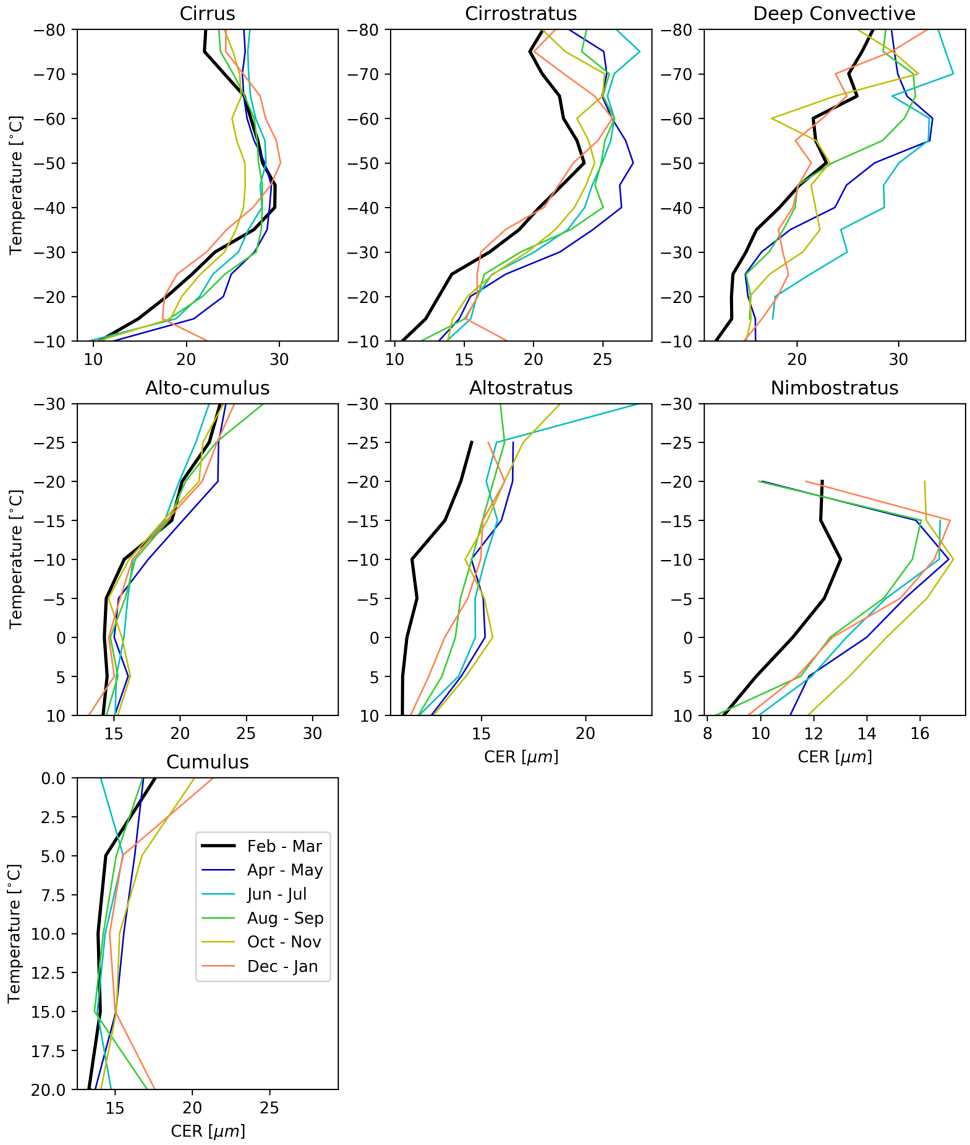

Figure 3-7: Relationship between Cloud Top Temperature and Cloud Effective Radius, for the cloud types defined by the ISCCP.

During Feb-Mar, CER is smaller for all differents cloud types compared to the other months, especially in altostratus and nimbostratus. Although the CER is the smallest during Feb-Mar for all cloud types, CWP is not necessarily the lowest. It is evident how CWP tends to be greater in alto-cumulus compared to the rest of the months, and slightly greater in cumulus, cirrus, and cirrostratus.

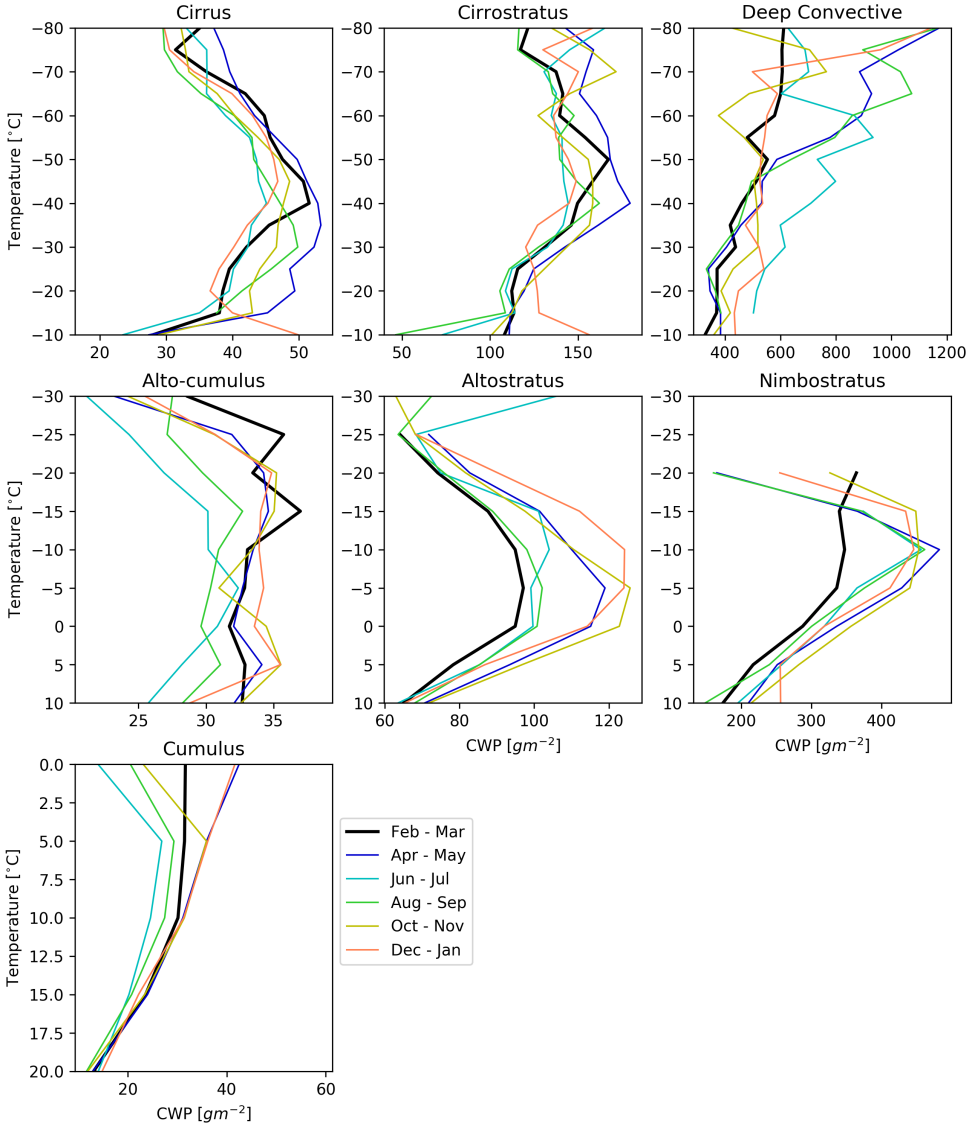

Figure 3-8: Relationship between Cloud Top Temperature and Cloud Water Path, for the cloud types defined by the ISCCP.

3.6. Aerosol-precipitation interaction over the Aburrá Valley

Rainfall in the Aburrá Valley results from dynamical combinations of local and synoptic patterns and thermodynamic features (Bedoya-Soto et al., 2019). The complex topography and hydroecological features of the valley make the study and forecasting of precipitation a major challenge on the geosciences' research topics. In the Aburrá valley, the diurnal cycle of rainfall is bimodal (Roldán-Henao et al., 2020), having one peak during the afternoon (from 1400 to 1700 LT) and a second peak during the night (from 0000 to 0400 LT). Afternoon precipitation in the valley typically presents as a cluster of small, but deep, convective systems with short life spans. Nocturnal precipitation is, on the other hand, characterized by low-intensity and long-lived stratiform systems.

This section studies aerosol-cloud-precipitation interactions in the Aburrá Valley from considering the thermodynamic and air quality conditions before afternoon rainfall events. We only considered afternoon events because unstable atmospheric conditions favor the ascent of pollutants and promote the interaction between aerosols, clouds, and precipitation.

For this, we estimated Moist Static Energy (MSE), Relative Humidity, and Potential Temperature Gradient (PTG) using the microwave radiometer measurements between 1100 LT and 1300 LT; we selected these hours because they correspond to the most convective conditions before the start of the precipitation event. PTG corresponds to the difference between the potential temperature in a level minus the upper level's potential temperature. MSE corresponds to a thermodynamic variable, analogous to equivalent potential temperature. It is calculated by lifting air, adiabatically, to the top of the atmosphere, and allowing for the condensation of all water vapor present in the air, thus releasing latent heat, as follows:

$$MSE = C_p T + gz + L_v r \tag{3-4}$$

where C_p is the specific heat at constant pressure for air, T is the absolute temperature,

g is the gravity acceleration, z is the height at a given reference level, and r is the vapor mixing ratio. Details are presented in Wallace and Hobbs (2006). Air quality data were obtained from a PM2.5 monitor located at Universidad Nacional de Colombia (see Figure **2-1**) between 0700 LT and 1000 LT.

The establishment of the thermodynamic thresholds obeys the following methodology:

1. We compared the difference between thermodynamic profiles for days with afternoon precipitation and the historical average. Figure **3-9**a,c and e show in magenta the MSE, Relative Humidity, and PTG during rainy days. As can be seen, before the onset of afternoon rainfall events, the atmospheric energy and humidity profiles are higher in all the atmospheric column compared to the mean values. Differences in PTG are only important between 800 and 700 hPa.

2. We selected the heights at which the differences between the thermodynamic profiles (Rainy days - mean) were greater at different altitudes. Figure **3-9**b,d, and f show the difference between rainy and mean days. The colored areas correspond to the selected regions.

3. To obtain the thresholds, we calculate the 10th, 20th, 30th and 40th percentiles of the distribution of the thermodynamic profiles during rainy days in the afternoon. In this way, it is warranted that 90, 80, 70, and 60 % of the afternoon rain events exceed this thermodynamic threshold.

Once thermodynamic thresholds were obtained, it was evaluated how the probability of rainfall occurrence changed with aerosol concentration variations. We only considered the days when all thermodynamic thresholds were exceeded.

Figure **3-10** presents the results. As can be seen, the probability of an afternoon rainfall occurrence in the Aburrá Valley increases with increasing aerosol concentration. This is especially clear for the 20th percentile in the thermodynamic threshold. However, we can

see this increment when aerosol concentration is greater than its 40th percentile (0.4 in the x-label of Figure **3-10**), which corresponds to a concentration of 22 μgm^{-3}.

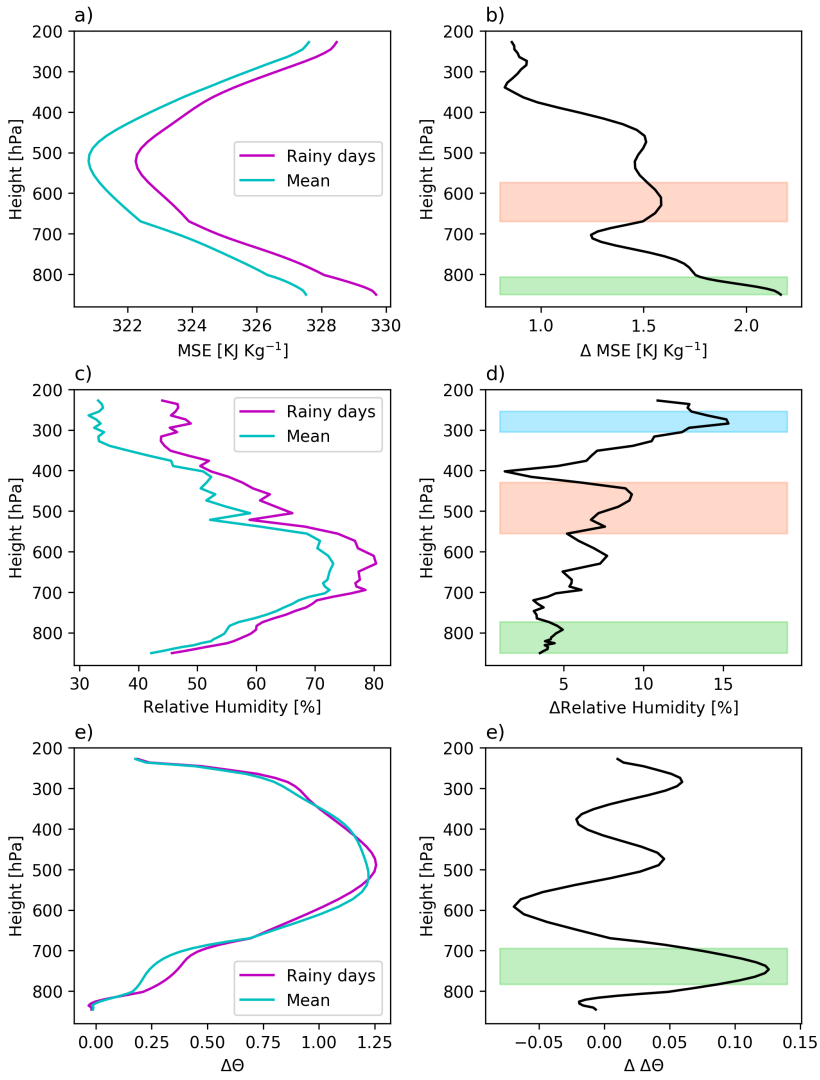

Figure 3-9: a) Moist Static Energy between 1100 LT and 1300 LT in the Aburrá Valley for days with aternoon raindall (magenta) and mean conditions (blue). c) The same as a) for Relative Humidity. e) The same as a) for Potential Temperature Gradient. b) Difference between Rainy days and mean curves in label a). The colored areas corresponds to the heights at which the difference is greater. d) The same as b) for Relative Himidity. f) The same as b) for Potential Temperature Gradient.

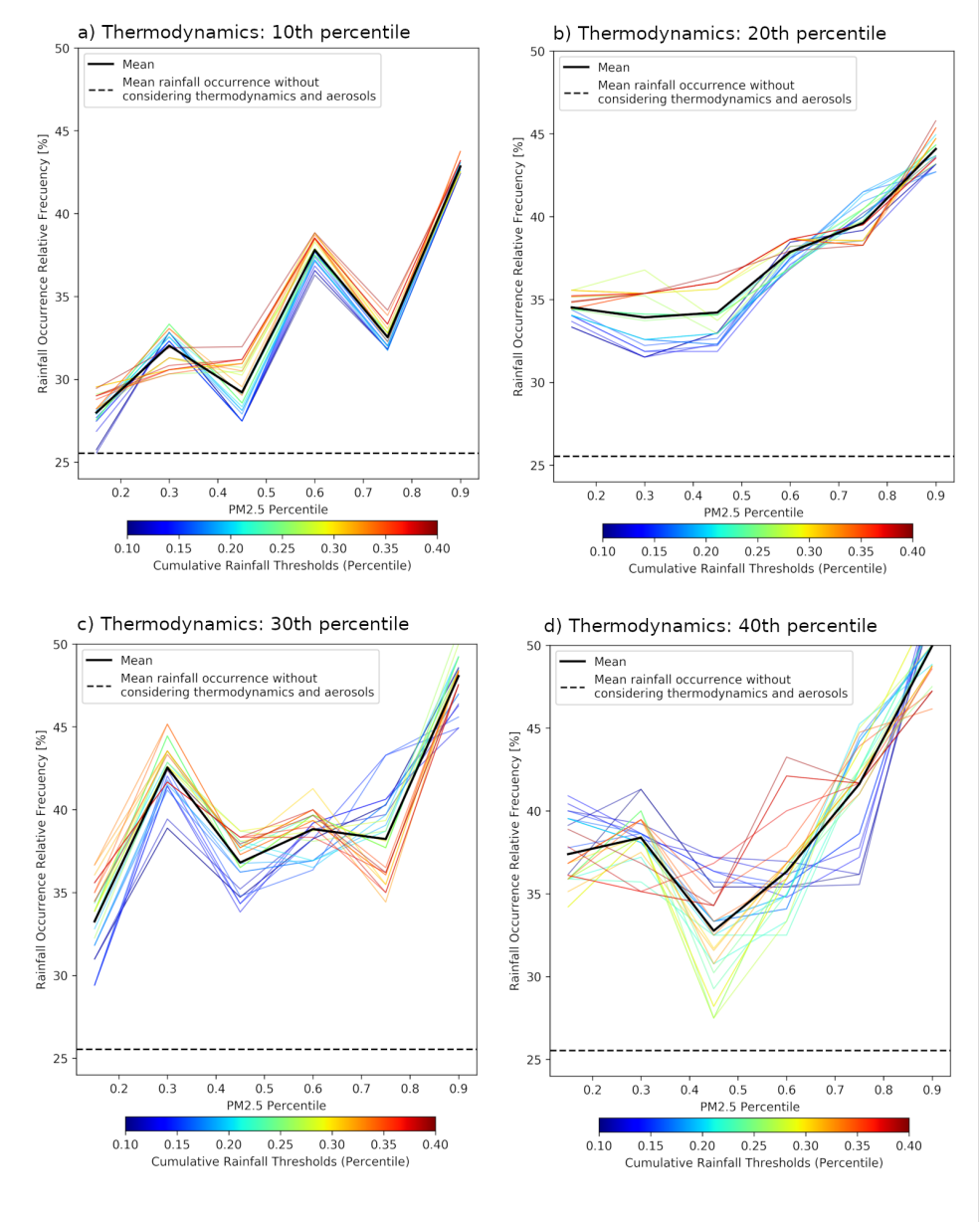

Figure 3-10: Probability of an afternoon rainfall occurrence as a function of PM2.5 percentiles, during days where thermodynamic thresholds were exceeded. Considering the thermodynamic threshold as the a) 10th, b) 20th, c) 30th, and d)40th percentiles.

Previous studies in the Aburrá Valley have found that the scavenging effect of precipitation on PM2.5 and PM10 are strongly dependent on the atmospheric stability. Hence daytime

precipitation in the Aburrá Valley induces near-surface stabilization, which in turn affects the dispersion processes and promotes aerosol accumulation near the surface (Roldán-Henao et al., 2020). Considering the evidence presented here, it is possible to suggest that a positive feedback exists between aerosols and precipitation in the Aburrá Valley. An increase in aerosol concentration during days where thermodynamic conditions are favorable for rain formation will increase the rainfall occurrence probability. The occurrence of a rainfall event in the afternoon will lead to an early stabilization of the atmosphere, which, combined with the city's local emissions, will favor aerosols' accumulation near the surface.

To conclude this section, we decided to investigate the differences between two afternoon-rainfall events in the Aburrá Valley. One during a clean day (February 20th, 2020, aerosol concentration lower than its 10th percentile) and another during a polluted day (February 26th, 2020, aerosol concentration higher than its 90th percentile). We took two days with similar thermodynamic conditions, so differences were associated with aerosol differences. Figure **3-11**a,b, and c) shows the MSE, Relative Humidity, and PTG ($\Delta\Theta$) between 1100 LT and 1300 LT for the clean (blue line) and polluted (magenta line) days. As can be seen, thermodynamic differences are negligible. Figure **3-11**d shows the rainfall rate and cumulative precipitation. In both days, precipitation lasted for around 2 hours, and the cumulative rainfall was similar, with approximately 5 mm. However, as shown in figures **3-11**e,f the February 26th event had intervals of greater intensity, that is, it was a more convective event. Further, as figure **3-11**g shows, the raindrops' size was smaller during the day with the higher aerosol concentration compared to the clean day.

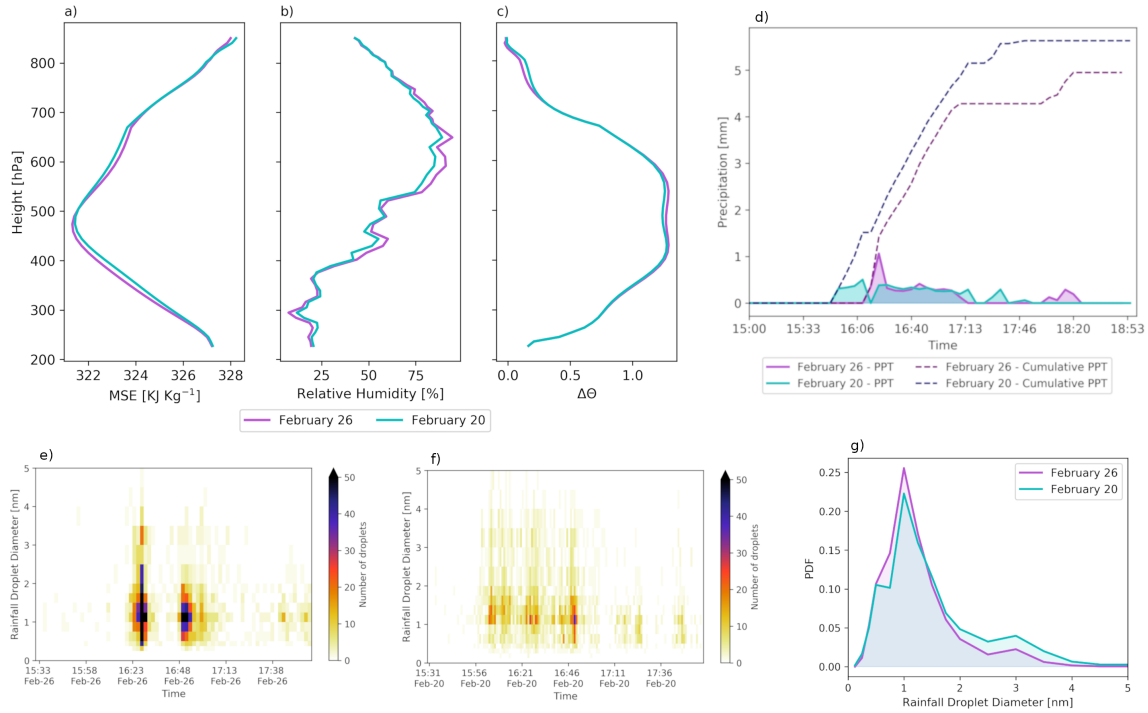

Figure 3-11: Case study of two afternoon-rainfall events in the Aburrá Valley, for a day with a high concentration of PM2.5 (February 26th, 2020) and a low concentration of PM2.5 (February 20th, 2020). a-c) Thermodynamic profiles between 1100 LT and 1300 LT for MSE, Relative Humidity, and Potential Temperature Gradient ($\Delta\Theta$), respectively. a) Rainfall rate and cumulative precipitation for both days. e-f) Time evolution of raindrops' size distribution for both days. g) Average raindrops' size distribution for both days.

3.6.1. Aerosol indirect effect assessment over Colombia

As mentioned before, to study aerosol indirect effect over Colombia territory, we decided to investigate Nd variations with aerosol load (AOD). Figure **3-12** present Nd in the north of South America for ice and liquid phase of clouds. In general, the interactions between aerosols and the ice phase of clouds are less well understood compared to the liquid phase. Likewise, there are multiple uncertainties in the calculation of Nd for ice clouds, for which the results presented here correspond to a first approach and require further work in the future.

As can be seen, the spatial variations of ice and liquid droplet concentration are quite similar in the north of South America. The main difference corresponds to the magnitude of the number of droplets, which is greater for the liquid phase. Nd is higher in the Peruvian and Ecuatorial coasts. When we look at the Colombia territory, Nd is slightly greater over the Andes mountain range.

When observing the spatial distribution of aerosols (see Figure **2-12**b) and Nd over Colombia, it is striking that the Andean zone tends to have the lowest concentration of aerosols. Nevertheless, it is the place where the highest Nd occurs. The formation, properties, and spatial distribution of clouds in Colombia are the result of multiple processes occurring in the local and regional scale, and in many cases, they co-occur. Colombian topography and the migration of the Intertropical Convergence Zone (ITCZ) modulate the cloud formation processes to a large extent, and therefore analyzing the spatial variations of these variables does not seem to be sufficient.

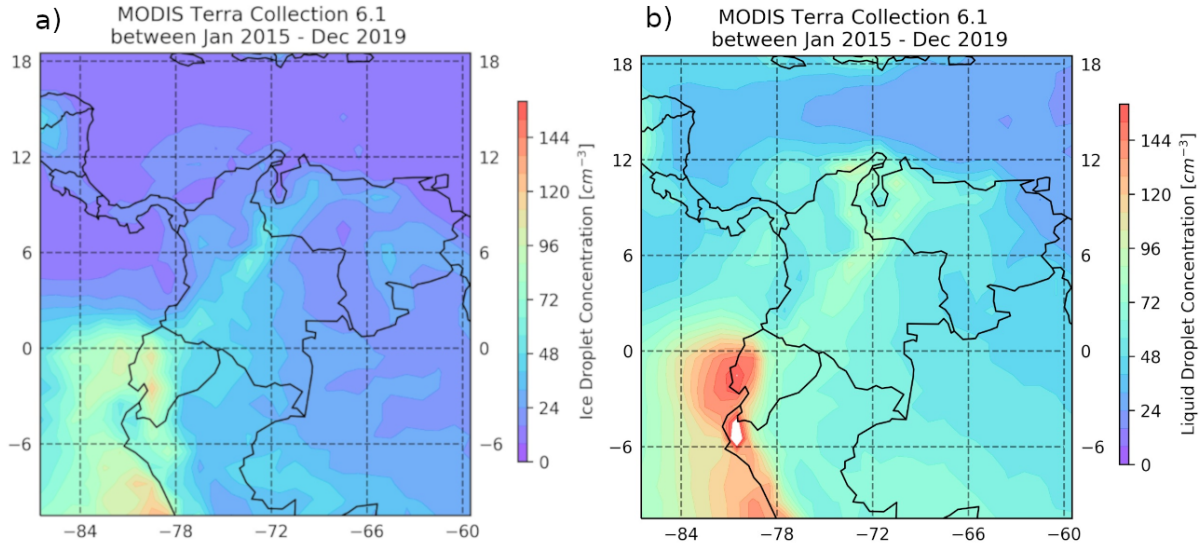

Figure 3-12: a) Ice droplet concentration in the North of South America between January 2015 and December 2019. b) the same as a) for liquid droplet concentration.

Figure **3-13** presents the variations of CER, Nd, and CWP probability distributions with AOD, for the liquid phase (a, c, and e) and the ice phase (b, d, and f) of clouds in the

North of South America. It is clear how the number of cloud droplets increases with AOD, but they decrease in size, just as The Twomey's theory states. It is notorious how the CWP decreases with the AOD for liquid clouds; however, there is no clear relationship between both variables in the ice phase.

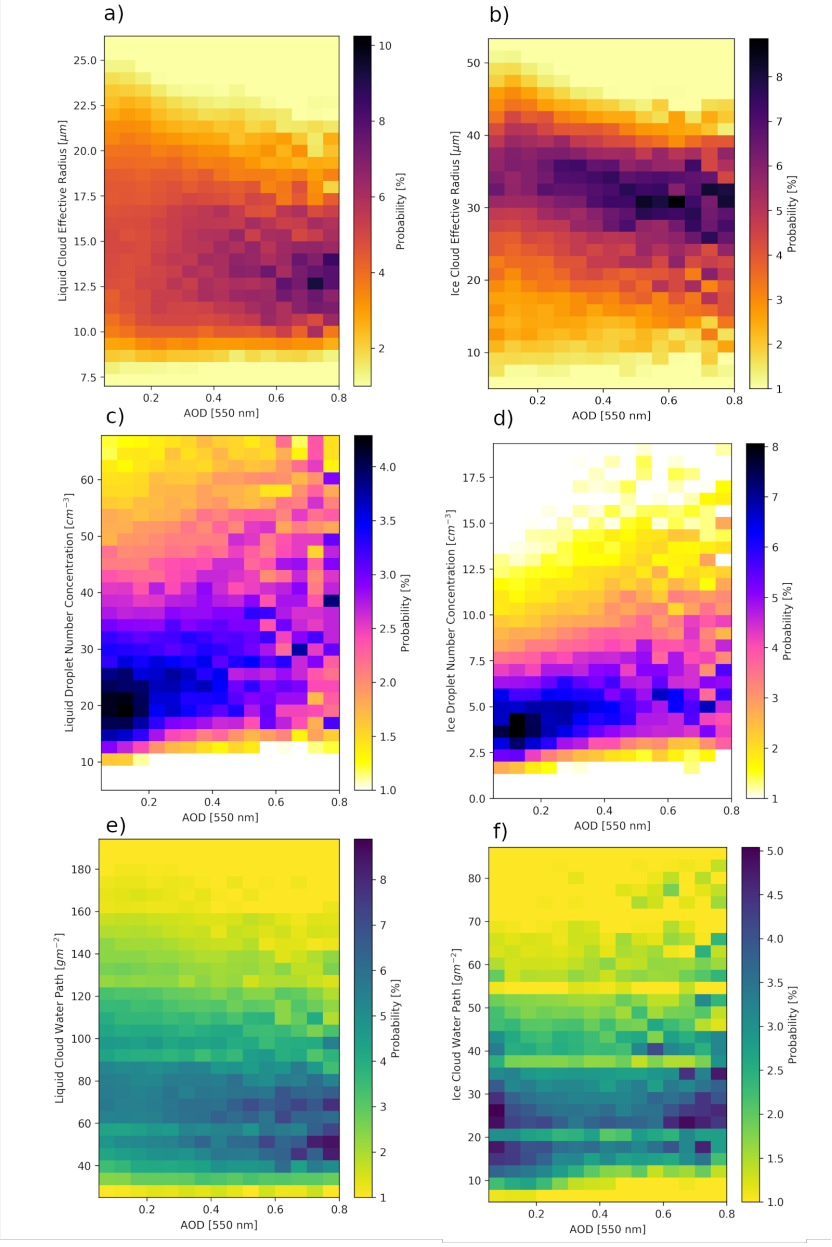

Figure 3-13: a, c, and e) Variations in the CER, Nd, and CWP probability distributions with AOD for the liqued phase of clouds. b, d, and f) Variations in the CER, Nd, and CWP probability distributions with AOD for the ice phase of clouds.

Finding a value that describes how much Nd varies with aerosol concentration is ideal for understanding and forecasting aerosols' impact on cloud formation. However, this value is frequently calculated as an average of the data set used. Which provides a reduced view of the phenomenon. In this section, we computed the rate between Nd and AOD following Feingold et al. (2001). This value is usually computed as an average of the dataset used. Nevertheless, in this section, we decided to calculate this value for the Cloud Droplet Concentration percentiles.

$$ACI_N = \frac{\Delta lnN_d}{\Delta ln\alpha}, 0 < ACI_N < 1 \tag{3-5}$$

Where α is the AOD, results for the liquid and ice phases are present in figure **3-14**. As can be seen, liquid $\Delta lnNd/\Delta lnAOD$ rate has a parabolic shape, with a maximum in the Nd's 30th percentile. In the case of the ice phase, the rate of $\Delta lnNd/\Delta lnAOD$ increases until it reaches the 90th percentile of the Nd, where this rate is reduced. It is relevant to consider that the interactions between aerosols and ice clouds are less well understood. Therefore, there are multiple uncertainties in the calculation of Nd for ice clouds. The results presented here correspond to a first attempt and can't be considered entirely true because it requires further work in the future.

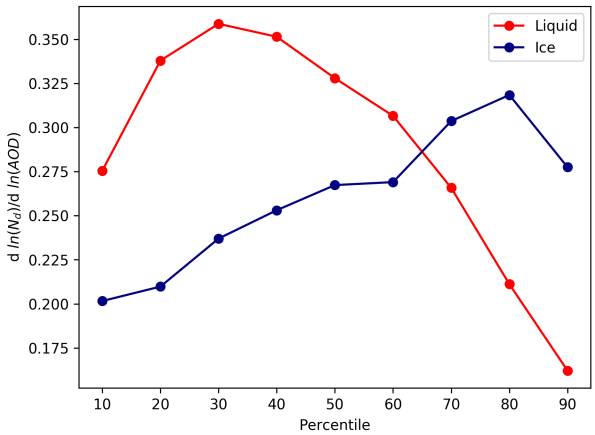

Figure 3-14: Rate of change of Nd with AOD as a function of Nd percentiles, for the liquid (red) and ice (blue) phases of clouds.

3.7. Final remarks

Aerosols are considered one of the most significant sources of uncertainties in global climate change. Their ability to modify cloud formation and precipitation patterns makes them one of the anthropogenic pollutants that most concern humanity. That is why aerosols are currently one of the main environmental issues studied on a global scale.

This study investigates aerosol indirect effect over the Aburrá Valley and Colombia, using ground-based and satellite information. The complex topography of the Aburrá Valley highly conditions cloud properties, especially cloud cover, cloud effective radius, and cloud temperature. In general, the cloud droplet effective radius in the Valley was highly dependent on their temperature (height) rather than the available water. That makes sense because, given the Valley's geographic location, the relative humidity remains high throughout the year, and therefore water is not usually a limiting resource. We found that CER increases linearly only for constant intervals of COT, and it is especially sensitive to water content when cloud droplets are small. Cloud effective radius increases with decreasing temperature, which allows the explanation of the main spatial differences in droplet size throughout the Valley.

Evidence suggests that aerosols could have significant impacts on cloud properties within the Valley. We found evidence that suggests that the diffusion process of convective clouds in the Valley could be retarded because of the high aerosol concentration during February and March. That could directly impact the convective precipitation that commonly occurs in the Aburrá Valley during the afternoon hours. Using a C-band weather radar, a microwave radiometer, and a PM2.5 monitor, we assessed aerosol-precipitation interactions in the Valley. We found that as PM2.5 increases in the Valley, the occurrence probability of afternoon-rainfall events increases. According to previous studies, after an afternoon-rainfall event in the Valley, PM2.5 concentration increases because of the induced near-surface stabilization and anthropogenic emissions. We concluded that an increase in afternoon-rainfall events in the Valley could create a positive feedback between aerosols and precipitation.

Finally, we investigated aerosol-cloud interactions in the north of South America (Colombia) using MODIS aerosol and cloud properties at 1-degree. We found that as aerosol concentration increase, the number of cloud droplets increase but with smaller sizes. For the liquid phase of clouds, CWP also decreases with increasing aerosols. However, for the ice phase, we could not found a clear relationship.

4 Conclusions

The high levels of pollution registered daily worldwide make the study, understanding, and forecasting of aerosol's effect on climate and meteorology completely necessary, especially when many people are currently susceptible to these changes. Despite this, aerosols today correspond to one of the main sources of uncertainty in global climate change.

This work corresponds to a first attempt to study aerosols' effect on the Aburrá Valley and Colombia territory. We found significant variations in local and regional meteorological conditions as a result of the aerosols' presence.

We started by characterizing aerosols within the Aburrá valley and found that they are mainly fine particles, with a diameter of less than 1 μm and high black carbon content. In the Aburrá Valley, aerosols interact with radiation through scattering and absorbing processes, which reduces the amount of solar radiation as much as -40 Wm^{-2} during the morning hours. We conclude that this reduction is not only a function of aerosol load but also of solar zenith angle.

Over the Colombian territory, biomass burning triggers most of the solar radiation reductions, which are especially high over the Caribean coast and the Orinoquia region, near Venezuela. These reductions could be higher than -45 Wm^{-2}.

In the Aburrá Valley, we also found reductions in latent and sensible fluxes due to aerosols' presence, which lead to changes in the atmospheric boundary layer height. For the latter, we found that aerosols inhibit the ABL Height's growth of up to 300 meters.

Aerosols also seem to modify cloud properties. As aerosols act as cloud condensation nucleis, they essentially change cloud droplets size and hence precipitation formation processes. With the use of satellite information, we investigated aerosols indirect effect over the Aburrá Valley and Colombia. We found that droplets' radius depends mainly on cloud top temperature, rather than water content, and is especially sensitive on the latter when cloud droplets are small.

We could investigate aerosol-precipitation interaction from thermodynamic profiles, precipitation derived by a C-band weather radar, and PM2.5 hourly concentration. We found that when thermodynamic conditions are sufficient for formating an afternoon-rainfall event in the Aburrá Valley, the probability of occurrence of an afternoon-rainfall event will increase if we increase the concentration of PM2.5 during the morning hours.

The results obtained here allow us to suggest that aerosols in the Aburrá Valley could potentially create two positive feedback processes. The first one results from the inhibition of the ABL height, which arise from the perturbation of incident solar radiation and energy fluxes. In this feedback process, the increased aerosol concentration will lead to a reduction in the height of the ABL, which in turn favors the accumulation of pollutants near the surface, leading to an increase in aerosols concentration. The second feedback results from the increased probability of occurrence of an afternoon-rainfall event with increasing aerosols. As mentioned, according to a previous study, afternoon-rainfall events increase particulate matter concentration in the Aburrá Valley (Roldán-Henao et al., 2020). Thus, an increase in aerosol concentration during morning hours will lead to an increase in afternoon-rainfall events, which favors aerosol accumulation near the surface.

Finally, it is necessary to conclude that future research is required to verify or reject these feedback processes suggested here. Which, if proven, could have profound impacts on the meteorological conditions of the Aburrá Valley.

Bibliografía

Albrecht, B. A. (1989). Aerosols, cloud microphysics, and fractional cloudiness. *Science*, 245(4923):1227–1230.

Altaratz, O., Koren, I., Remer, L., and Hirsch, E. (2014). Cloud invigoration by aerosols—coupling between microphysics and dynamics. *Atmospheric Research*, 140:38–60.

Andreae, M. O., Rosenfeld, D., Artaxo, P., Costa, A., Frank, G., Longo, K., and Silva-Dias, M. A. F. d. (2004). Smoking rain clouds over the amazon. *science*, 303(5662):1337–1342.

Arakawa, A. and Schubert, W. H. (1974). Interaction of a cumulus cloud ensemble with the large-scale environment, part i. *Journal of the Atmospheric Sciences*, 31(3):674–701.

Atwater, M. A. (1970). Planetary albedo changes due to aerosols. *Science*, 170(3953):64–66.

Bedoya-Soto, J. M., Aristizábal, E., Carmona, A. M., and Poveda, G. (2019). Seasonal shift of the diurnal cycle of rainfall over medellin's valley, central andes of colombia (1998–2005). *Frontiers in Earth Science*, 7:92.

Bell, T. L., Rosenfeld, D., Kim, K.-M., Yoo, J.-M., Lee, M.-I., and Hahnenberger, M. (2008). Midweek increase in us summer rain and storm heights suggests air pollution invigorates rainstorms. *Journal of Geophysical Research: Atmospheres*, 113(D2).

Boucher, O., Randall, D., Artaxo, P., Bretherton, C., Feingold, G., Forster, P., Kerminen, V.-M., Kondo, Y., Liao, H., Lohmann, U., et al. (2013). Clouds and aerosols. In *Climate change 2013: the physical science basis. Contribution of Working Group I to the Fifth*

Assessment Report of the Intergovernmental Panel on Climate Change, pages 571–657. Cambridge University Press.

Boucher, O., Schwartz, S. o., Ackerman, T., Anderson, T., Bergstrom, B., Bonnel, B., Chỳlek, P., Dahlback, A., Fouquart, Y., Fu, Q., et al. (1998). Intercomparison of models representing direct shortwave radiative forcing by sulfate aerosols. *Journal of Geophysical Research: Atmospheres*, 103(D14):16979–16998.

Boucher, O. and Tanré, D. (2000). Estimation of the aerosol perturbation to the earth's radiative budget over oceans using polder satellite aerosol retrievals. *Geophysical research letters*, 27(8):1103–1106.

Braslau, N. and Dave, J. (1973). Effect of aerosols on the transfer of solar energy through realistic model atmospheres. part i: Non-absorbing aerosols. *Journal of applied meteorology*, 12(4):601–615.

Bréon, F.-M., Tanré, D., and Generoso, S. (2002). Aerosol effect on cloud droplet size monitored from satellite. *Science*, 295(5556):834–838.

Cess, R., Potter, G., Ghan, S., and Gates, W. (1985). The climatic effects of large injections of atmospheric smoke and dust: A study of climate feedback mechanisms with one-and three-dimensional climate models. *Journal of Geophysical Research: Atmospheres*, 90(D7):12937–12950.

Chandra, S., Dwivedi, A. K., and Kumar, M. (2014). Characterization of the atmospheric boundary layer from radiosonde observations along eastern end of monsoon trough of India. *Journal Earth Syst. Sci*, 123(6):1233–1240.

Charlock, T. P. and Sellers, W. D. (1980). Aerosol effects on climate: Calculations with time-dependent and steady-state radiative-convective models. *Journal of the atmospheric sciences*, 37(6):1327–1341.

Charlson, R. and Pilat, M. (1969). Climate: The influence of aerosols. *Journal of Applied Meteorology*, 8(6):1001–1002.

Christensen, M. W., Chen, Y.-C., and Stephens, G. L. (2016). Aerosol indirect effect dictated by liquid clouds. *Journal of Geophysical Research: Atmospheres*, 121(24):14–636.

Christopher, S. A. and Zhang, J. (2002). Shortwave aerosol radiative forcing from modis and ceres observations over the oceans. *Geophysical Research Letters*, 29(18):6–1.

Coakley, J. A., Bernstein, R. L., and Durkee, P. A. (1987). Effect of ship-stack effluents on cloud reflectivity. *Science*, 237(4818):1020–1022.

Coakley Jr, J. A., Cess, R. D., and Yurevich, F. B. (1983). The effect of tropospheric aerosols on the earth's radiation budget: A parameterization for climate models. *Journal of the Atmospheric Sciences*, 40(1):116–138.

De Wekker, S. F. J. and Kossmann, M. (2015). Convective Boundary Layer Heights Over Mountainous Terrain—A Review of Concepts. *Frontiers in Earth Science*, 3:77.

DePuy, V., Berger, V. W., and Zhou, Y. (2014). Wilcoxon-mann-whitney test: Overview. *Wiley StatsRef: Statistics Reference Online*.

Dubovik, O., Holben, B., Eck, T. F., Smirnov, A., Kaufman, Y. J., King, M. D., Tanré, D., and Slutsker, I. (2002). Variability of absorption and optical properties of key aerosol types observed in worldwide locations. *Journal of the atmospheric sciences*, 59(3):590–608.

Emeis, S., Schäfer, K., Münkel, C., Friedl, R., and Suppan, P. (2012). Evaluation of the interpretation of ceilometer data with rass and radiosonde data. *Boundary-layer meteorology*, 143(1):25–35.

Fan, J., Rosenfeld, D., Zhang, Y., Giangrande, S. E., Li, Z., Machado, L. A., Martin, S. T., Yang, Y., Wang, J., Artaxo, P., et al. (2018). Substantial convection and precipitation enhancements by ultrafine aerosol particles. *Science*, 359(6374):411–418.

Feingold, G., Remer, L. A., Ramaprasad, J., and Kaufman, Y. J. (2001). Analysis of smoke impact on clouds in brazilian biomass burning regions: An extension of twomey's approach. *Journal of Geophysical Research: Atmospheres*, 106(D19):22907–22922.

Feingold, G., Stevens, B., Cotton, W., and Walko, R. (1994). An explicit cloud microphysics/les model designed to simulate the twomey effect. *Atmospheric Research*, 33(1-4):207–233.

Freitas, S. R., Longo, K. M., Dias, M. A. S., Dias, P. L. S., Chatfield, R., Prins, E., Artaxo, P., Grell, G. A., and Recuero, F. S. (2005). Monitoring the transport of biomass burning emissions in south america. *Environmental Fluid Mechanics*, 5(1-2):135–167.

García, O., Díaz, A., Expósito, F., Díaz, J., Dubovik, O., Dubuisson, P., Roger, J.-C., Eck, T., Sinyuk, A., Derimian, Y., et al. (2008). Validation of aeronet estimates of atmospheric solar fluxes and aerosol radiative forcing by ground-based broadband measurements. *Journal of Geophysical Research: Atmospheres*, 113(D21).

García, O., Díaz, J., Expósito, F., Díaz, A., Dubovik, O., Dubuisson, P., Roger, J.-C., et al. (2012). Shortwave radiative forcing and efficiency of key aerosol types using aeronet data. *Atmospheric Chemistry and Physics*, 12(11):5129.

Garrett, T., Zhao, C., Dong, X., Mace, G., and Hobbs, P. (2004). Effects of varying aerosol regimes on low-level arctic stratus. *Geophysical Research Letters*, 31(17).

Gobbi, G., Kaufman, Y., Koren, I., and Eck, T. (2007). Classification of aerosol properties derived from aeronet direct sun data.

Grosvenor, D. P., Sourdeval, O., Zuidema, P., Ackerman, A., Alexandrov, M. D., Bennartz, R., Boers, R., Cairns, B., Chiu, J. C., Christensen, M., et al. (2018). Remote sensing of droplet number concentration in warm clouds: A review of the current state of knowledge and perspectives. *Reviews of Geophysics*, 56(2):409–453.

Guzman, G. (2018). Analisis de la influencia del diseño urbano en la meteorologia del valle de aburra. Master's thesis, Universidad Nacional de Colombia - Sede Medellín.

Hansen, J. E. and Travis, L. D. (1974). Light scattering in planetary atmospheres. *Space science reviews*, 16(4):527–610.

Herrera-Mejía, L. and Hoyos, C. D. (2019a). Characterization of the atmospheric boundary layer in a narrow tropical valley using remote-sensing and radiosonde observations and the WRF model: the Aburrá Valley case-study. *Quarterly Journal of the Royal Meteorological Society*, 0(0).

Herrera-Mejía, L. and Hoyos, C. D. (2019b). Characterization of the atmospheric boundary layer in a narrow tropical valley using remote-sensing and radiosonde observations and the wrf model: the aburrá valley case-study. *Quarterly Journal of the Royal Meteorological Society*, 145(723):2641–2665.

Holanda, B. A., Pöhlker, M. L., Saturno, J., Sörgel, M., Ditas, J., Ditas, F., Wang, Q., Donth, T., Artaxo, P., Barbosa, H. M., et al. (2020). Influx of african biomass burning aerosol during the amazonian dry season through layered transatlantic transport of black carbon-rich smoke. *Atmospheric Chemistry and Physics*, 20(8):4757–4785.

Hoyos, C. D., Herrera-Mejía, L., Roldán-Henao, N., and Isaza, A. (2020). Effects of fireworks on particulate matter concentration in a narrow valley: the case of the medellín metropolitan area. *Environmental Monitoring and Assessment*, 192(1):6.

Hulst, H. C. and van de Hulst, H. C. (1981). *Light scattering by small particles*. Courier Corporation.

Jacobson, M. Z. (2001). Strong radiative heating due to the mixing state of black carbon in atmospheric aerosols. *Nature*, 409(6821):695–697.

Jia, H., Ma, X., Yu, F., Liu, Y., and Yin, Y. (2019). Distinct impacts of increased aerosols on cloud droplet number concentration of stratus/stratocumulus and cumulus. *Geophysical Research Letters*, 46(22):13517–13525.

Kaufman, Y. J. (1993). Aerosol optical thickness and atmospheric path radiance. *Journal of Geophysical Research: Atmospheres*, 98(D2):2677–2692.

King, M. D., Menzel, W. P., Kaufman, Y. J., Tanré, D., Gao, B.-C., Platnick, S., Ackerman, S. A., Remer, L. A., Pincus, R., and Hubanks, P. A. (2003). Cloud and aerosol proper-

ties, precipitable water, and profiles of temperature and water vapor from modis. *IEEE Transactions on Geoscience and Remote Sensing*, 41(2):442–458.

Kleinman, L. I., Daum, P. H., Lee, Y.-N., Lewis, E. R., Sedlacek III, A., Senum, G., Springston, S., Wang, J., Hubbe, J., Jayne, J., et al. (2012). Aerosol concentration and size distribution measured below, in, and above cloud from the doe g-1 during vocals-rex. *Atmospheric Chemistry and Physics*, 12(1):207.

Koren, I., Kaufman, Y. J., Remer, L. A., and Martins, J. V. (2004). Measurement of the effect of amazon smoke on inhibition of cloud formation. *Science*, 303(5662):1342–1345.

Koren, I., Kaufman, Y. J., Rosenfeld, D., Remer, L. A., and Rudich, Y. (2005). Aerosol invigoration and restructuring of atlantic convective clouds. *Geophysical Research Letters*, 32(14).

Lacagnina, C., Hasekamp, O. P., and Torres, O. (2017). Direct radiative effect of aerosols based on parasol and omi satellite observations. *Journal of Geophysical Research: Atmospheres*, 122(4):2366–2388.

Lacis, A. A. and Hansen, J. (1974). A parameterization for the absorption of solar radiation in the earth's atmosphere. *Journal of the atmospheric sciences*, 31(1):118–133.

Levy, R., Mattoo, S., Munchak, L., Remer, L., Sayer, A., Patadia, F., and Hsu, N. (2013). The collection 6 modis aerosol products over land and ocean. *Atmospheric Measurement Techniques*, 6(11):2989.

Li, Z., Guo, J., Ding, A., Liao, H., Liu, J., Sun, Y., Wang, T., Xue, H., Zhang, H., and Zhu, B. (2017). Aerosol and boundary-layer interactions and impact on air quality. *National Science Review*, 4(6):810–833.

Loeb, N. G. and Kato, S. (2002). Top-of-atmosphere direct radiative effect of aerosols over the tropical oceans from the clouds and the earth's radiant energy system (ceres) satellite instrument. *Journal of Climate*, 15(12):1474–1484.

Loeb, N. G. and Manalo-Smith, N. (2005). Top-of-atmosphere direct radiative effect of aerosols over global oceans from merged ceres and modis observations. *Journal of climate*, 18(17):3506–3526.

Loeb, N. G., Manalo-Smith, N., Kato, S., Miller, W. F., Gupta, S. K., Minnis, P., and Wielicki, B. A. (2003). Angular distribution models for top-of-atmosphere radiative flux estimation from the clouds and the earth's radiant energy system instrument on the tropical rainfall measuring mission satellite. part i: Methodology. *Journal of applied meteorology*, 42(2):240–265.

Loeb, N. G. and Su, W. (2010). Direct aerosol radiative forcing uncertainty based on a radiative perturbation analysis. *Journal of climate*, 23(19):5288–5293.

Lotteraner, C. and Piringer, M. (2016). Mixing-Height Time Series from Operational Ceilometer Aerosol-Layer Heights. *Boundary-Layer Meteorology*, 161(2):265–287.

Mann, H. B. and Whitney, D. R. (1947). On a test of whether one of two random variables is stochastically larger than the other. *The annals of mathematical statistics*, pages 50–60.

Matus, A. V., L'Ecuyer, T. S., Kay, J. E., Hannay, C., and Lamarque, J.-F. (2015). The role of clouds in modulating global aerosol direct radiative effects in spaceborne active observations and the community earth system model. *Journal of Climate*, 28(8):2986–3003.

McCormick, R. A. and Ludwig, J. H. (1967). Climate modification by atmospheric aerosols. *Science*, 156(3780):1358–1359.

Mendez-Espinosa, J., Belalcazar, L., and Betancourt, R. M. (2019). Regional air quality impact of northern south america biomass burning emissions. *Atmospheric environment*, 203:131–140.

Molinié, J. and Pontikis, C. (1995). A climatological study of tropical thunderstorm clouds and lightning frequencies on the french guyana coast. *Geophysical research letters*, 22(9):1085–1088.

Münkel, C. and Roininen, R. (2010). Automatic monitoring of boundary layer structures with ceilometers. *Vaisala News*, 184.

Myhre, G. (2009). Consistency between satellite-derived and modeled estimates of the direct aerosol effect. *Science*, 325(5937):187–190.

Nakajima, T., Higurashi, A., Kawamoto, K., and Penner, J. E. (2001). A possible correlation between satellite-derived cloud and aerosol microphysical parameters. *Geophysical Research Letters*, 28(7):1171–1174.

Nakajima, T. and King, M. D. (1990). Determination of the optical thickness and effective particle radius of clouds from reflected solar radiation measurements. part i: Theory. *Journal of the atmospheric sciences*, 47(15):1878–1893.

Nemesure, S., Wagener, R., and Schwartz, S. E. (1995). Direct shortwave forcing of climate by the anthropogenic sulfate aerosol: Sensitivity to particle size, composition, and relative humidity. *Journal of Geophysical Research: Atmospheres*, 100(D12):26105–26116.

North, G. R., Pyle, J. A., and Zhang, F. (2014). *Encyclopedia of atmospheric sciences*, volume 1. Elsevier.

Patadia, F., Gupta, P., and Christopher, S. A. (2008). First observational estimates of global clear sky shortwave aerosol direct radiative effect over land. *Geophysical research letters*, 35(4).

Pawlowska, H. and Brenguier, J.-L. (2000). Microphysical properties of stratocumulus clouds during ace-2. *Tellus B*, 52(2):868–887.

Penner, J., Charlson, R., Hales, J., Laulainen, N., Leifer, R., Novakov, T., Ogren, J., Radke, L., Schwartz, S., and Travis, L. (1994). Quantifying and minimizing uncertainty of climate forcing by anthropogenic aerosols. *Bulletin of the American Meteorological Society*, 75(3):375–400.

Platnick, S., King, M. D., Ackerman, S. A., Menzel, W. P., Baum, B. A., Riédi, J. C., and Frey, R. A. (2003). The modis cloud products: Algorithms and examples from terra. *IEEE Transactions on Geoscience and Remote Sensing*, 41(2):459–473.

Quaas, J., Boucher, O., Bellouin, N., and Kinne, S. (2008). Satellite-based estimate of the direct and indirect aerosol climate forcing. *Journal of Geophysical Research: Atmospheres*, 113(D5).

Radke, L. F., Coakley, J. A., and King, M. D. (1989). Direct and remote sensing observations of the effects of ships on clouds. *Science*, 246(4934):1146–1149.

Rajeev, K. and Ramanathan, V. (2001). Direct observations of clear-sky aerosol radiative forcing from space during the indian ocean experiment. *Journal of Geophysical Research: Atmospheres*, 106(D15):17221–17235.

Ramanathan, V., Crutzen, P., Kiehl, J., and Rosenfeld, D. (2001). Aerosols, climate, and the hydrological cycle. *science*, 294(5549):2119–2124.

Reid, J. S. and Hobbs, P. V. (1998). Physical and optical properties of young smoke from individual biomass fires in brazil. *Journal of Geophysical Research: Atmospheres*, 103(D24):32013–32030.

Roldán-Henao, N., Hoyos, C. D., Herrera-Mejía, L., and Isaza, A. (2020). An investigation of the precipitation net effect on the particulate matter concentration in a narrow valley: Role of lower troposphere stability. *Journal of Applied Meteorology and Climatology*, (2020).

Rosenfeld, D. (1999). Trmm observed first direct evidence of smoke from forest fires inhibiting rainfall. *Geophysical research letters*, 26(20):3105–3108.

Rosenfeld, D. (2000). Suppression of rain and snow by urban and industrial air pollution. *Science*, 287(5459):1793–1796.

Rosenfeld, D., Andreae, M. O., Asmi, A., Chin, M., de Leeuw, G., Donovan, D. P., Kahn, R., Kinne, S., Kivekäs, N., Kulmala, M., et al. (2014). Global observations of aerosol-cloud-precipitation-climate interactions. *Reviews of Geophysics*, 52(4):750–808.

Rosenfeld, D. and Gutman, G. (1994). Retrieving microphysical properties near the tops of potential rain clouds by multispectral analysis of avhrr data. *Atmospheric research*, 34(1-4):259–283.

Rosenfeld, D., Kaufman, Y., and Koren, I. (2006). Switching cloud cover and dynamical regimes from open to closed benard cells in response to the suppression of precipitation by aerosols.

Rosenfeld, D. and Lensky, I. M. (1998). Satellite-based insights into precipitation formation processes in continental and maritime convective clouds. *Bulletin of the American Meteorological Society*, 79(11):2457–2476.

Rosenfeld, D., Lohmann, U., Raga, G. B., O'Dowd, C. D., Kulmala, M., Fuzzi, S., Reissell, A., and Andreae, M. O. (2008). Flood or drought: how do aerosols affect precipitation? *science*, 321(5894):1309–1313.

Rossow, W., Mosher, F., Kinsella, E., Arking, A., Desbois, M., Harrison, E., Minnis, P., Ruprecht, E., Seze, G., Simmer, C., et al. (1985). Isccp cloud algorithm intercomparison. *Journal of Climate and Applied Meteorology*, 24(9):877–903.

Schuster, G. L., Dubovik, O., and Holben, B. N. (2006). Angstrom exponent and bimodal aerosol size distributions. *Journal of Geophysical Research: Atmospheres*, 111(D7).

Seinfeld, J. H. and Pandis, S. N. (2012). *Atmospheric chemistry and physics: from air pollution to climate change*. John Wiley & Sons.

Sepúlveda, J. (2015). Estimación cuantitativa de precipitación a partir de la información de radar meteorológico del área metropolitana del valle de aburrá. Master's thesis, Universidad Nacional de Colombia - Sede Medellín.

Sepúlveda, J. and Hoyos, C. D. (2017). Disdrometer-based C-Band Radar Quantitative Precipitation Estimation (QPE) in a highly complex terrain region in tropical Colombia. *AGU Fall Meeting Abstracts*.

Shi, S., Cheng, T., Gu, X., Guo, H., Wu, Y., and Wang, Y. (2019). Biomass burning aerosol characteristics for different vegetation types in different aging periods. *Environment international*, 126:504–511.

Stull, R. B. (1988). *An Introduction to Boundary Layer Meteorology*, volume 13. Springer.

Su, W., Loeb, N. G., Schuster, G. L., Chin, M., and Rose, F. G. (2013). Global all-sky shortwave direct radiative forcing of anthropogenic aerosols from combined satellite observations and gocart simulations. *Journal of Geophysical Research: Atmospheres*, 118(2):655–669.

Tao, W.-K., Chen, J.-P., Li, Z., Wang, C., and Zhang, C. (2012). Impact of aerosols on convective clouds and precipitation. *Reviews of Geophysics*, 50(2).

Twomey, S. et al. (1974). Pollution and the planetary albedo. *Atmos. Environ*, 8(12):1251–1256.

Universidad Pontificia Bolivariana and Área Metropolitana del Valle de Aburrá (2017). Inventario de emisiones atmosféricas del Valle de Aburrá, actualización 2015. Technical report, Área Metropolitana del Valle de Aburrá, Medellín.

Wallace, J. M. and Hobbs, P. V. (2006). *Atmospheric science: an introductory survey*, volume 92. Elsevier.

Weare, B. C., Temkin, R. L., and Snell, F. M. (1974). Aerosol and climate: some further considerations. *Science*, 186(4166):827–828.

Werner, F., Ditas, F., Siebert, H., Simmel, M., Wehner, B., Pilewskie, P., Schmeissner, T., Shaw, R., Hartmann, S., Wex, H., et al. (2014). Twomey effect observed from collocated microphysical and remote sensing measurements over shallow cumulus. *Journal of Geophysical Research: Atmospheres*, 119(3):1534–1545.

Whiteman, C. D., Hoch, S. W., Horel, J. D., and Charland, A. (2014). Relationship between particulate air pollution and meteorological variables in Utah's Salt Lake Valley. *Atmospheric Environment*, 94:742–753.

Young, D., Minnis, P., Doelling, D., Gibson, G., and Wong, T. (1998). Temporal interpolation methods for the clouds and the earth's radiant energy system (ceres) experiment. *Journal of Applied Meteorology*, 37(6):572–590.

Yu, H., Kaufman, Y., Chin, M., Feingold, G., Remer, L., Anderson, T., Balkanski, Y., Bellouin, N., Boucher, O., Christopher, S., et al. (2006). A review of measurement-based assessments of the aerosol direct radiative effect and forcing.

Yu, H., Liu, S., and Dickinson, R. E. (2002). Radiative effects of aerosols on the evolution of the atmospheric boundary layer. *Journal of Geophysical Research: Atmospheres*, 107(D12):AAC–3.

Yu, H., Liu, S. C., and Dickinson, R. E. (2001). Radiative effects of aerosols on the evolution of the atmospheric boundary layer. *Journal of Geophysical Research: Atmospheres*, 107(D12):AAC 3–1–AAC 3–14.

Zhang, Y., Gao, Z., Li, D., Li, Y., Zhang, N., Zhao, X., and Chen, J. (2014). On the computation of planetary boundary-layer height using the bulk Richardson number method. *Geoscientific Model Development*, 7(6):2599–2611.